Stress Coupling Between Earthquakes in Northwest Turkey and the North Aegean Sea

Süleyman S. Nalbant

Geophysics Department, Engineering Faculty, Istanbul University, Istanbul, Turkey

Aurélia Hubert and Geoffrey C. P. King

Laboratoire de Tectonique et Mécanique de la Lithosphère (UMR 7578 CNRS), Institut de Physique du Globe, Paris

Abstract. We have investigated the Coulomb stress interactions of 29 earthquakes ($M_s \geq 6.0$) that have occurred in the region of northwest Turkey and north Aegean Sea since 1912. Of these events, 23 may be related to earlier events, and 16 are clearly related to earlier events. All events after 1967 are related to previous events. Events in the early part of our time interval that show no correlation could be related to historical events as yet unidentified. In some cases, faults that have received a stress reduction from earlier events are prepared for an event by an earthquake occurring a few years before that creates a local Coulomb stress rise. Thus regions of Coulomb stress shadow can become regions where a damaging earthquake may occur. The relation between smaller events and the Coulomb stress distribution is less clear, but may be related to poor data quality and practical limitations of our modeling technique. Nonetheless, there are 4 times as many events per unit area in regions of enhanced stress than where stress is reduced. We discuss the contemporary distribution of Coulomb stress and argue that it is possible to identify the likely locations of future damaging earthquakes including identifying the most likely candidate faults.

1. Introduction

Over the last 5 years a series of papers have been published that investigate how earthquakes transfer stress. The studies divide into two broad categories, although some publications include both. One category concentrates on the correlation between a large event and the subsequent small events and tends to examine relatively short time periods [*Harris and Simpson*, 1992; *Stein et al.*, 1992; *King et al.*, 1994b; *Stein et al.*, 1994; *Harris et al.*, 1995; *Hodgkinson et al.*, 1996*; Nalbant et al.*, 1996; *Jacques et al.*, 1996] while the other category looks at the interactions between larger events and has necessarily looked at longer time scales [*Stein et al.*, 1992; *Reasenberg and Simpson*, 1992; *King et al.*, 1994b; *Harris and Simpson*, 1996; *Jaumé and Sykes*, 1996; *Stein et al.*, 1997; *Deng and Sykes*, 1997; *Nostro et al.*, 1997].

This study is mainly concerned with the interactions between large events and over long time periods. We examine the region of western Turkey and the north Aegean (Figure 1) where 29 large events have occurred since 1912. By combining tectonic information and field reports we can adequately define the earlier events, while later instrumental studies mean that more recent events are well constrained. Their mechanisms are certainly well enough determined to show that the effects of interaction can be seen throughout the period. Of particular interest is the observation that the interaction covers a two-dimensional area and is not restricted to a single fault zone such as that, farther to the east, studied by *Stein et al*. [1997]. None of the source mechanisms are as well constrained as recent events in California nor are small earthquakes as well located; consequently, the relation between the large events and small events is not as clear as in regions where the data is better.

2. Tectonic Setting

In the area studied, the deformation is related to the Aegean back arc extension and to the North Anatolian Fault [*Barka*, 1992; *Armijo et al.*, 1996]. The extension started between 15 and 10 Ma and produced several major east-west normal fault systems in western Anatolia and the Aegean. The North Anatolian Fault is a major strike-slip fault nearly 1500 km in length extending from eastern Turkey to the Gulf of Corinth associated with the westward extrusion of Anatolia. It seems to have been born 10

Myr ago in eastern Turkey following the collision of Arabian and the Eurasian plate. Westward growth then followed with preexisting fault systems being modified as the propagating fault tip arrived [*Armijo et al*., 1996]. Deep troughs such as the Sea of Marmara, the North Aegean Trough, the Skyros Basin, and the Gulf of Corinth (Figures 1 and 2) are a major consequence of this process. The continuing deformation processes can be seen from repeated Global Positioning System (GPS) measurements in Turkey and the Aegean [*Oral et al.*, 1995; *Reilinger et al.*, 1997] and by the rupture of 950 km of the North Anatolian fault between 1939 and 1967 in a sequence of earthquakes of magnitude greater than 7 [*Ketin*, 1969].

The stress interaction of this latter sequence has been investigated by *Stein et al*. [1997], who found that the initiation of all but one of the six events could be explained by stresses resulting from the preceding deformation history. Our study extends their work to the west. At the eastern extremity of our area (between 32°E and 30.7°E) the North Anatolian Fault is a single, though segmented feature, with some minor secondary faults to the north in the Duzce Basin (Figures 1 and 2). The 1944, 1957 and 1967 earthquakes of the North Anatolian Fault sequence, studied by *Stein et al*. [1997], are also included in this study. They resulted in slip on all the fault segments in that region. As the North Anatolian Fault starts to interact with the extensional environment of the Aegean, it splits into two main branches composed of en echelon segments with linking pull-apart basins. The northern branch is predominant. It forms the deep Marmara Sea basins and crosses the northern edge of the Gelibolu Peninsula to reach the Gulf of Saros and the North Aegean Trough (Figures 1 and 2). The southern branch is less clear in the morphology. It bounds the southern edge of several lakes south of the Sea of Marmara then turns southwest crossing the Biga Peninsula and reaches the Gulf of Edremit and the Skyros Basin (Figures 1 and 2). It can be traced as far as the Euboia Island and is mechanically linked to the Gulf of Corinth [see *Armijo et al*., 1996]. Around the Sea of Marmara, a dense GPS network was established which gives a slip rate on the North Anatolian Fault of 17 ± 3 mm/yr [*Straub and Khale*, 1995; *Straub*, 1996].

Since the shear deformation associated with the North Anatolian fault predominates, it is not surprising that most events are predominantly right-lateral strike-slip in character (Figure 3), but the geometry of the fault system resulting from the propagation processes results in some events having a substantial normal component and even, in a few cases, a significant component of reverse faulting. As illustrated by Figure 1 the seismic activity is not restricted to the North Anatolian Fault system. To the south there is a transition to north-south extension associated with the Bakircay, Simav, Gediz and Eskisehir normal fault zones [*Ambraseys and Tchalenko*, 1972; *Arpat and* Bingöl, 1969; *Angelier et al.*, 1981; *Westaway*, 1990]. The focal mechanisms associated with these grabens of Western Anatolia indicate almost pure normal faulting (Figure 3).

As remarked in section 1, it is evident that the interactions between the different events must be more complex in character than those occurring along the simple-shear North Anatolian Fault to the east.

3. Coulomb stress Interaction

To look at stress interaction between faults, we follow the overall approach taken by *Reasenberg and Simpson* [1992] and *King et al*. [1994b], who model faults as discontinuities in an elastic half-space. Following *King et al*., [1994b], optimum fault angles are calculated using the stress field created by adding a regional stress field to that induced by dislocations representing the faults and computing the directions that maximize the Coulomb failure stress:

$$\sigma_f = \tau - \mu' \sigma_n \quad (1)$$

where σ_n and τ are the effective normal stress and shear stress on these optimum planes and μ' the effective friction coefficient. The change in failure criterion is then the change in $\Delta\sigma_f$:

$$\Delta\sigma_f = \Delta\tau - \mu' \Delta\sigma_n \quad (2)$$

where $\Delta\tau$ and $\Delta\sigma_n$ are changes in the shear and normal stresses on these planes.

The use of an effective friction μ' is a way to allow for the unknown effects of fluid pressure. In dry rock, μ' could be as great as 0.75 and with sufficient fluid over pressure could fall to 0.0. For a normal faulting region, neither exceptional fluid pressure nor dry conditions are plausible. We therefore select the intermediate value of 0.4. *King et al*. [1994b] point out that even substantial variations from such a value do not greatly alter the distribution of Coulomb stresses around a fault and *Stein et al*. [1997] indicate that in general, the changes in absolute values are not great either. In this study the information about source moment is limited, and commensurately, our ability to determine the amplitudes of stress

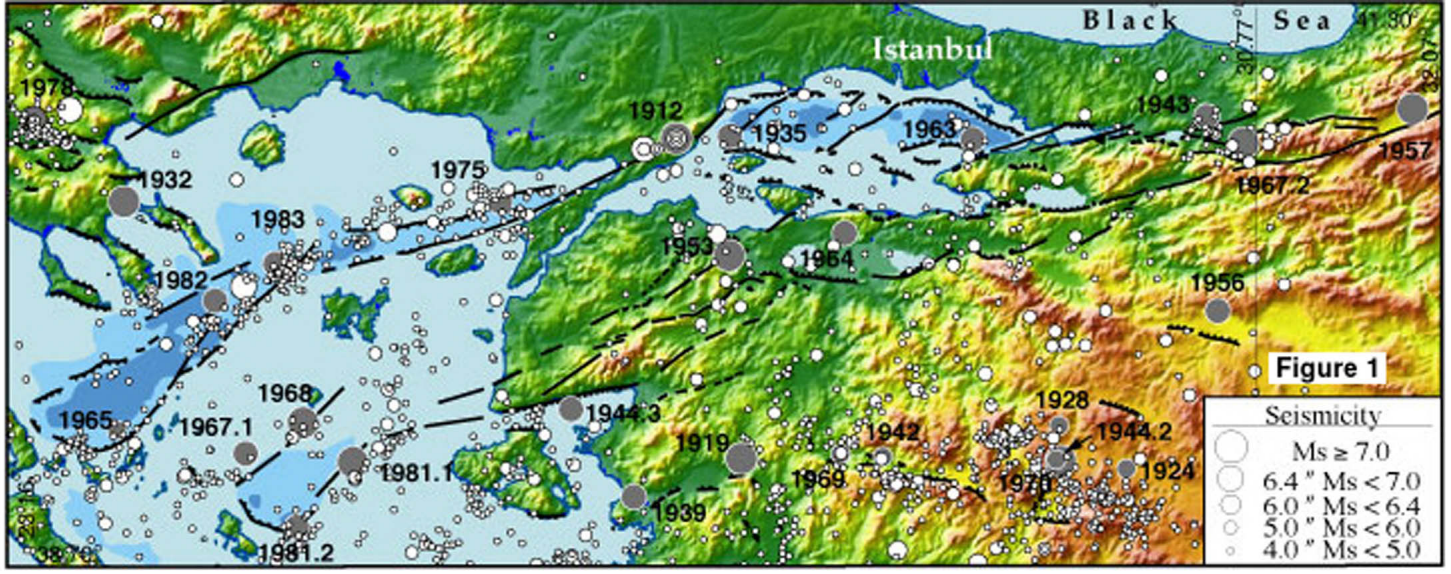

Tectonic map of western Turkey and the north Aegean Sea with the seismicity between 1900 and 1996. Gray circles indicate the epicenters of the earthquakes used to calculate the Coulomb stress evolution from 1912 to 1996. See Figure 1 for geographical information.

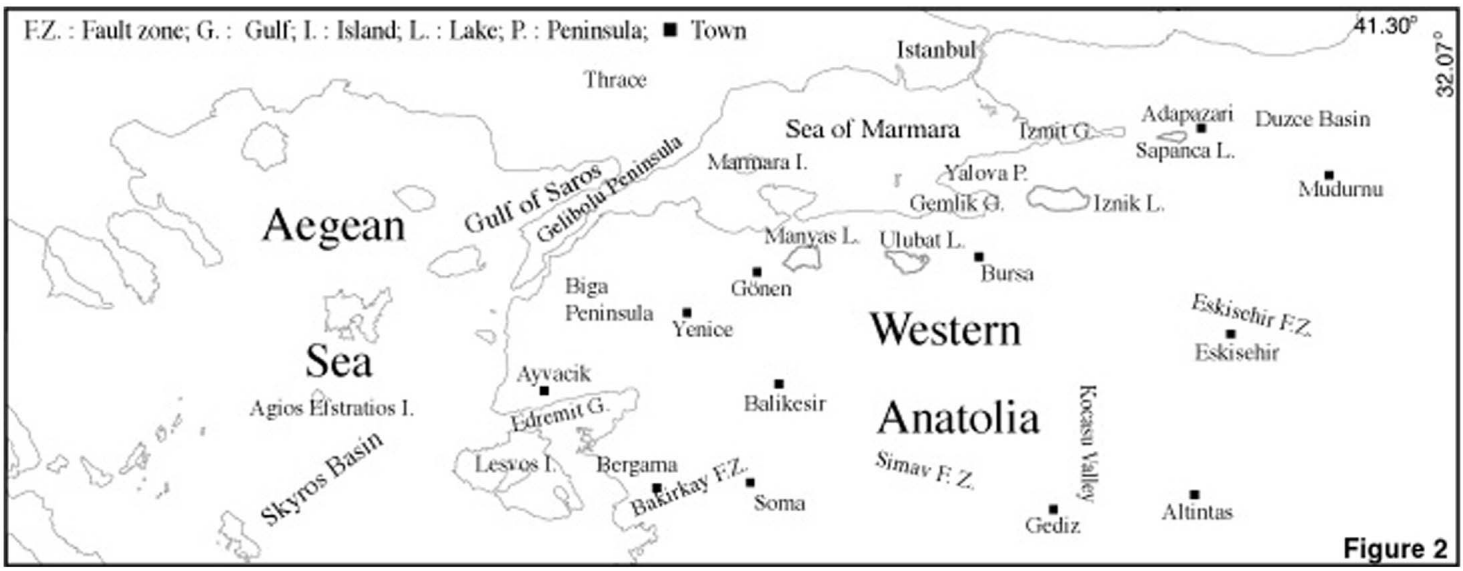

Geographical locations used in the text.

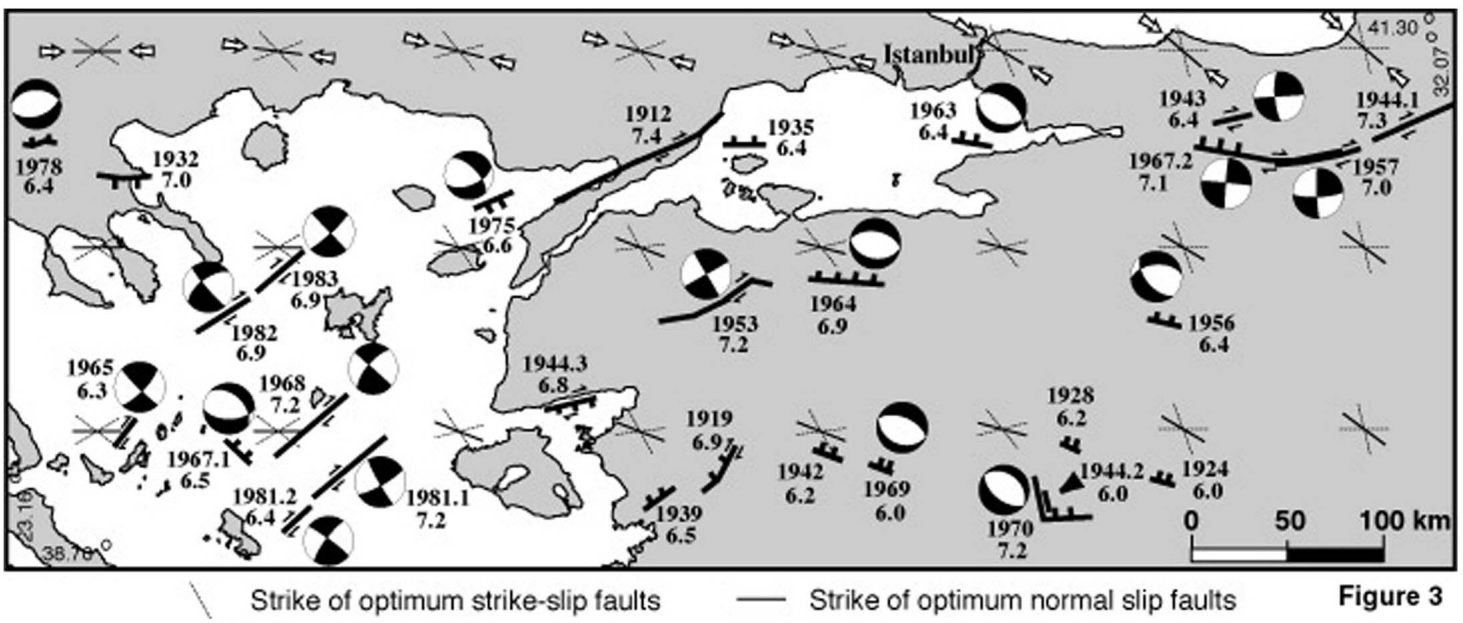

Faults used to model of the earthquakes studied with those focal available mechanisms (lower hemisphere). The regional stress pattern used and the resulting optimum orientations for normal and strike-slip faults are also shown. The date and the magnitude (Ms) of each earthquake are indicated.

changes. Thus, within a range of possible values (0.2-0.6) our assumptions about effective friction are not a source of significant error. This insensitivity also means that our data cannot be used to constrain values of effective friction.

Coulomb stresses are calculated for depths of 6.5 km, and the seismogenic thickness is taken to be 12.5 km. There is not much information to constrain these values. However, in the Aegean region, reliably located aftershocks recorded with local networks are rarely much deeper than 12.5 km [*King et al.*, 1985; *Soufleris et al.*, 1982]. This is similar to maximum earthquake depths for much of central California where it can also be shown that although small earthquakes occur throughout the seismogenic zone, most seismic moment is released at depths near to its center [*King et al.*, 1994a].

The Coulomb stress distribution depends on the earthquake mechanism and close to a fault is sensitive to details of the rupture. At a distance from the fault such detail is unimportant, and a distributed source is indistinguishable from a point source. This occurs at distances great compared to the fault dimensions. Fault dip information is also lost, and because of the free surface boundary condition only the components of the source moment tensor that have principal axes parallel and perpendicular to the free surface cause stresses at a distance. This is true for all long wavelength radiation from a shallow source [e.g., *Aki and Richards*, 1980]. We consider only the zero frequency component. In fact, only the horizontal component of slip at the source matters at such distances, and in the case of the 1912 event (where we are undecided about the dip direction for the reasons discussed in the appendix) we model the contractional component of the slip vector by a closure vector normal to a vertical fault plane. Unlike the other fault parameters, the Coulomb distribution is sensitive to both fault strike and the relative components of strike-slip and dip-slip motion. If the strike direction is changed (by $\leq 15°$) the shape of the distribution remains almost the same but is rotated by a similar amount to the change of strike. If the strike-slip component of the slip vector is changed relative to the horizontal component of the slip vector, a rotation also occurs which is similar in magnitude to the arctangent of the changed ratio. In the Coulomb distributions that we present below, these parameters only affect events that lie close to a transition from positive to negative Coulomb stress change. For our data, uncertainties of strike direction and the ratio of strike-slip to dip-slip motion do not result in rotations greater than $\pm 15°$ (except where specifically noted), and thus the effect of errors can be directly assessed by looking at Plates 1-10.

4. Earthquake Data

All the earthquakes that we have included in this study had magnitudes (M_s) ≥ 6.0, so we consider that they ruptured the full seismogenic layer. Thus vertical faults have a width (W) of 12.5 km, while nonvertical faults have widths that depend on their dips.

The information about the earthquakes is heterogeneous in nature, and since the descriptions of the events are in the appendix, we place the events into six categories. These roughly correspond to quality but also indicate differences in the type of data available. In the best category (Q = A) there are six events (1978, 1970, 1967.2, 1957, 1953, 1944.1) which occurred on land, and in each case we have a reliable fault plane solution and documented surface rupture associated with a fault exhibiting Holocene activity. For these events the fault parameters are unequivocal. For three older events (Q = B: 1944.2, 1932, 1912), fault plane solutions are not available, but well-documented surface ruptures associated with preexisting fault morphology allows the fault length, geometry, and the slip vector to be constrained. For four events (Q = C: 1969, 1964, 1956, 1943) the surface rupture information is poor or nonexistent. However, the focal mechanism, the epicentral location, the macroseismic data and the intensity mapped in the area can be used to associate the events with Holocene faults and hence define rupture plane(s), slip vector amplitude(s) and direction(s). For nine events that occurred beneath the sea, information is more limited (Q = D: 1983, 1982, 1981.2, 1981.1, 1975, 1968, 1967.1, 1965, 1963). Fortunately, all of these events have occurred since the installation of the World-Wide Standard Seismograph Network, and hence we have information concerning focal mechanisms and magnitudes which can be supplemented using aftershock distributions and bathymetric information. In category E there are four events (1944.3, 1942, 1939, 1935) for which the only information available is the epicentral location, the macroseismic zone and the magnitude. However, in each case they are located near active faults with clear fault morphology, so we can propose with some confidence the probable fault rupture. Finally, three events (Q = F: 1928, 1924, 1919) are apparently not located on a well-known fault system, so we model them using the characteristics of the nearest fault system (fault orientation and slip vector direction).

In categories C, D, E and F, empirical relations of *Kanamori and Anderson* [1975] are used to calculate

rupture parameters when field data are absent. The fault length (L, in km) is given by

$$\log L = M_s/2 - 2 \quad (3)$$

the moment (M_o, in N m) by

$$\log M_o = 1.5M + 9.1 \quad (4)$$

with $M = M_s$ and the displacement (u, in m) by

$$u = M_o /(L W\ 3.3\times10^{10}) \quad (5)$$

where W is the downdip width. The relations were also used in other cases (Q = A, B) to confirm that the field data are consistent with estimated event magnitudes.

Where we lack detailed information we have taken pure dip-slip events to have a mean dip of 45°. All the normal focal mechanisms are consistent with this mean value except for the 1970 Gediz earthquake where waveform modeling indicates a dip of 35°. Waveform modeling of the 1963 and 1975 events [*Taymaz et al.*, 1991] which have a combination of strike-slip and normal motion gives dips nearer to 60° so for all the oblique ruptures we assume a dip of 60°. We pointed out earlier, however, that the models are only sensitive to dip close to the fault. Thus a correct dip is only important for examining small earthquakes near to a major event and not the interactions between large events. The final parameters used for modeling the events are shown in Table 1. Several of the ruptures modeled are composed of segments with different strikes or slip vectors to best approximate the observations.

The epicentral location of the events and a tectonic map are shown in Figire 1 and available focal mechanisms are shown in Figure 3. Figure 3 also shows the location and the extent of surface ruptures that we have used to model the events. Their locations, surface wave magnitudes (M_s) and the focal mechanisms are also listed in Table 2. For convenience of referencing in figures and plates and in the text, we refer to both an earthquake and the associated fault by the year (e.g., 1912 earthquake or 1912 fault). Where more than one event has occurred in a year they are numbered in order of occurrence (e.g., 1981.1 and 1981.2).

5. Regional stress Direction

For Coulomb modeling, we need to know the most favored fault orientations. This is provided to the program by supplying a regional stress direction. The choice of directions of the principal axes is not critical within perhaps 15° [*King et al.*, 1994b], and there is little difficulty in establishing stress directions to this accuracy in our area. There are well-constrained fault slip data [*Zanchi and Angelier*, 1993] and earthquake focal mechanism solutions [*Müller et al.*, 1992; *Rebai et al.*, 1992]. GPS data have also been used to find the principal axis of extension and the orientation of the maximum shear stress around the Sea of Marmara [*Straub and Khale*, 1994, 1995]. These independent sets of data all suggest a mean N40°E extension direction for the Sea of Marmara that gradually changes in the west to become N-S in the north Aegean Sea. We use these results to define the stress field in the area and have modified the program reported in earlier papers [e.g., *King et al.*, 1994b] to take account of a varying stress field. The σ_{11}, σ_{33} and σ_{13} are defined on a grid of points and interpolated between them. The resulting normal and strike-slip optimum fault orientations and σ_1 directions are shown in Figure 3.

6. Coulomb Stress Modeling

We have calculated the static stress changes due to 29 earthquakes of $M \geq 6$ in the north Aegean Sea and western Turkey since 1912. Ideally, we would present 29 separate figures but this is not practical. If we assume, however, that there is no significant interaction between distant events, this allows us to divide the time period into nine stages which we show on Plates 1-9. The Coulomb stress changes are calculated for both optimally oriented strike-slip faults and normal faults since the events are normal or strike-slip or a combination of both. The maximum of either of the two fields gives the field of maximum stress change [*Hodgkinson et al.*, 1996] and it is this which we represent in Plates 1-10. We observe a stronger correlation between Coulomb stress increase on optimal strike-slip faults where this results in a pure strike-slip event and between Coulomb stress increase on optimal normal faults that move in purely normal events. Again it is not possible to include the number of figures necessary to demonstrate this, although where we quote values of Coulomb stress change we quote the appropriate value for the fault concerned.

In each Plate the faults that have moved are indicated by black lines enclosed by a white outline. Faults where the Coulomb stress is increased by more than 0.1×10^5 Pa (= 0.1 bar) are indicated by red lines enclosed by a black outline. We choose this limit as some previous studies suggest that a clear correlation only exists between a Coulomb stress change greater than 0.1×10^5 Pa and the subsequent earthquake activity [*Reasenberg and Simpson*, 1992; *Stein et al*., 1992]. However, as we remark in section 7, there may be a correlation with smaller Coulomb stress increases.

Faults where the Coulomb stress is decreased by more than 0.1×10^5 Pa are indicated by blue lines enclosed by a black outline. Faults where the Coulomb stress change is between $\pm 0.1 \times 10^5$ Pa are shown as single black lines. In each plate we have plotted the seismicity (Turkish catalogues) down to magnitude 3.0 as circles. Since it is useful distinguish between background seismicity and aftershocks, the former are shown as open circles and the latter as solid circles. As there is no certain criterion for selecting aftershocks, we define it to include all of the seismicity that occurs for a 12-month period in the region around the main shock. In Plates 6 and 7 it was not possible to select a single time window for the background seismicity since we include several major events in each plate. In those cases, temporal and spatial windows of background seismicity (Figure 4) were selected so that they represent regions that we can reasonably assume are most affected by the Coulomb stress changes. It is important to appreciate that the small events are not well located and that location accuracy varies both temporally and spatially. In general, more recent events are better located than earlier ones and bigger events are better located than smaller ones, (because they are recorded on more stations). Epicentral mislocations of 20 km are possible, and this defect of the data should be bourne in mind when assessing correlations.

7. Interaction Between the Major Events

Plates 1-9 illustrate the Coulomb stress interactions between the modeled earthquakes. Plate 1 shows the effects of the 1912, 1919 and 1924 events. The 1912 earthquake increased the stress on the 1975 fault by $0.05\text{-}1.0 \times 10^5$ Pa, the stress on the 1935 normal rupture by $0.1\text{-}1.0 \times 10^5$ Pa, the stress on the 1953 fault by $0.1\text{-}0.3 \times 10^5$ Pa and the stress on the 1964 fault by 0.1×10^5 Pa. It slightly decreased the stress on the eastern extremity of the 1944.3 fault by $0.1\text{-}0.2 \times 10^5$ Pa. The 1912 earthquake (M_s=7.4) is the first and the largest event modeled. Consequently, its stress change greatly influences our conclusions. However, it ruptures a major well-known fault (see the appendix) and the Coulomb stress pattern cannot be modified a lot. If the rupture is shorter or if the modelled reverse component occurred on the fault dipping toward the north or the south, the 1935, 1975 and 1953 earthquakes are still loaded by more than 0.1×10^5 Pa. The information we have on the 1919 and the 1924 events is limited. The location and the mechanism for the 1919 earthquake that we have chosen increase the Coulomb stress on the future 1939 event by $0.3\text{-}1.0 \times 10^5$ Pa. Even if we substantially change the strike and the slip direction of the 1919 event (M_s=6.9), the 1939 fault, which is located less than 20 km to the west (in the center of a red lobe), should still be loaded by it. The 1942 fault is located 30-35 km away in a region of no significant Coulomb stress increase. However, if the 1919 event ruptured a fault differing in strike by 15° (an E-W normal fault is the most likely), the Coulomb stress could have increased by up to 0.2×10^5 Pa. We might even conclude that this observation favors such an alternative mechanism for the 1919 event. The small 1924 earthquake (Ms=6.0) does not increase the stress on faults that rupture in later events (1928, 1944.2) by more than 0.1×10^5 Pa. However they do all experience stress increases.

In Plate 2 the Coulomb stress changes due to the 1928, 1932, 1935, 1939, 1942, 1943 and the 1944.1 events are added. The 1935 event decreases the stress on the 1953 fault; only the eastern extremity of the fault remains in a condition of increased stress ($> 0.1 \times 10^5$ Pa). However, three earthquakes of magnitude > 5 occur in the red lobe near the 1953 fault. The 1939 event slightly increases the Coulomb stress on the 1944.3 fault whose western extremity is no longer in a region of decreased Coulomb stress. The very large 1944.1 fault rupture, which extends east of our study area, was loaded by previous earthquakes still farther east on the North Anatolian Fault [*Stein et al*., 1996]. Together with the 1943 event it raises the stress by $0.5\text{-}5.0 \times 10^5$ Pa on the 1957 fault and by $0.5\text{-}1.0 \times 10^5$ Pa on the 1967 fault. The 1932 earthquake increases stress on the 1978 fault by $0.2\text{-}0.4 \times 10^5$ Pa. The 1942 event adds $0.1\text{-}0.3 \times 10^5$ Pa on the 1969 fault located less then 25 km to the east.

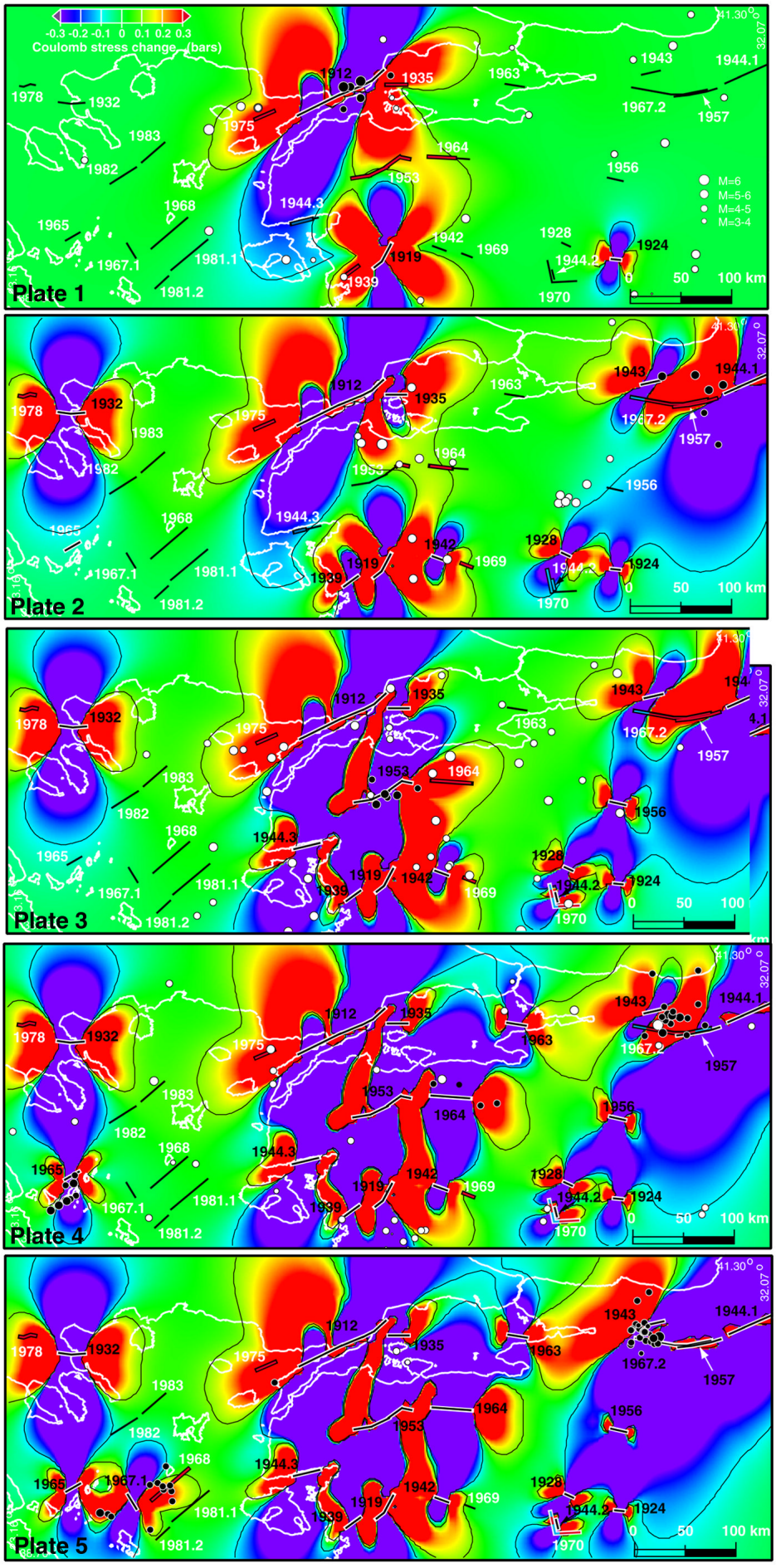
-0.3 -0.2 -0.1 0 0.1 0.2 0.3
Coulomb stress change (bars)
M=6
M=5-6
M=4-5
M=3-4
0 50 100 km
Plate 1
Plate 2
Plate 3
Plate 4
Plate 5
1912
1935
1963
1943
1944.1
1978
1932
1975
1967.2
1957
1983
1964
1982
1953
1956
1968
1944.3
1965
1942
1928
1969
1924
1967.1
1981.1
1919
1944.2
1939
1970
1981.2

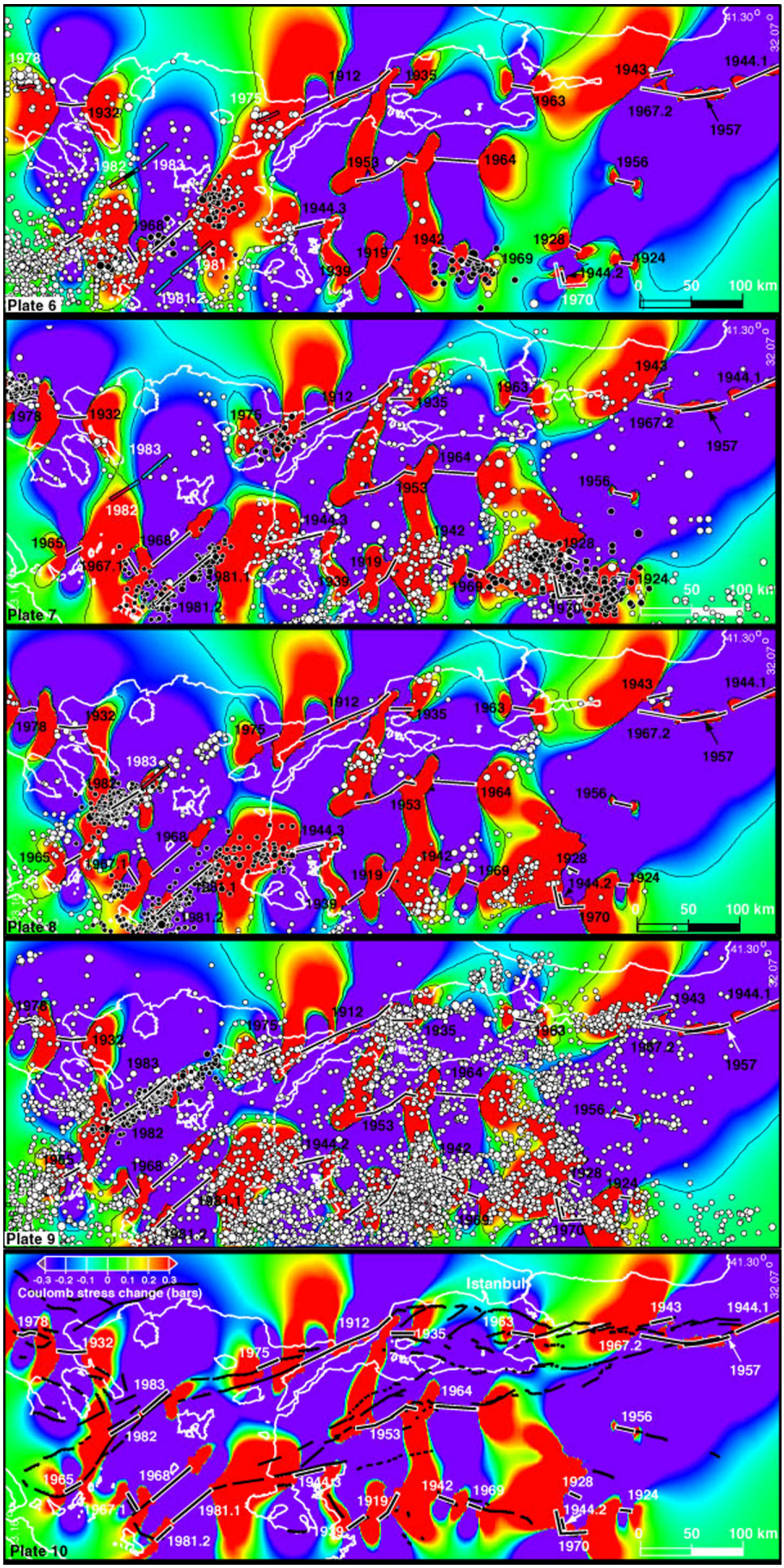
Plate 6
Plate 7
Plate 8
Plate 9
Plate 10
Istanbul
Coulomb stress change (bars)
-0.3 -0.2 -0.1 0 0.1 0.2 0.3
0 50 100 km
41.30°
32.07°
1978
1932
1975
1912
1935
1943
1944.1
1963
1967.2
1957
1983
1982
1953
1964
1956
1944.3
1968
1942
1928
1919
1969
1924
1981
1939
1944.2
1981.2
1970
1965
1967.1
1981.1

Plate Captions: **Plate 1.** Calculated Coulomb stress change on optimally oriented strike-slip, and normal faults caused by the 1912, 1919 and 1924 earthquakes with the background activity (open circles) between the 1935 and 1944.1 events. The ends of the color bar are pointed to indicate that the levels of mapped stress extend outside those shown in the bar. The faults that have moved are showed by black lines enclosed by a white outline. stress loaded faults are red, enclosed by a black outline. The faults in stress shadows are shown by blue lines enclosed by a black outline. Faults that are not affected by more than $\pm 0.1 \times 10^5$ Pa are represented by black lines. Subsequent plates adopt the same conventions as described above. Notice that the 1912 event strongly loads the 1935 and the 1975 faults, and adds some load to the 1953 and the 1964 faults. The 1912 aftershocks are plotted with solid circles. The 1939 fault is loaded by the 1919 earthquake.

Plate 2. Coulomb stress change due to the previous events plus those in 1928, 1932, 1935, 1939, 1942, 1943 and 1944.1. The background activity (open circles) between the 1935 and the 1944.1 events is also shown. The 1932 event loads the 1978 fault in the northern part of the Aegean. The 1939 earthquake releases the 1919 stress increase and adds load on the 1944.3 fault. Slip on the 1944.1 and 1943 faults strongly loads the 1957 and 1967 faults preparing them to slip. The 1944.1 aftershocks are plotted with solid circles.

Plate 3. Coulomb stress change due to the previous events plus the 1944.2, 1944.3, 1953 and 1956 events. The background activity (open circles) between the 1944.1 and 1963 events is shown. The 1944.2 rupture adds load on the 1970 fault. The 1964 fault is loaded by the 1953 event whose aftershock activity (solid circles) fits with the Coulomb stress increase. Slip on the 1957 fault further increases the stress level in the region where the future 1967.2 event will occur.

Plate 4. Coulomb stress change due to the previous events plus those in 1957, 1963, 1964 and 1965. The background activity (open circles) between the 1963 and 1967.1 events is also shown. The 1957 earthquake strongly increases stress on the 1967 fault previously loaded by the 1944.1 and 1943. The aftershock activity (solid circles) is located at the western end of the rupture zone. The 1964 rupture transfers the 1953 stress increase farther to the east, loading the fault system south of Ulubat lake. The 1963 event loads the west part of the Sea of Marmara close to Istanbul.

Plate 5. Coulomb stress change due to the previous events plus those in 1967.1 and 1967.2. The background seismicity (open circles) between the 1967.1 and 1968 events is also shown. The 1967.1 event loads the nearby 1968 and 1981 faults. The 1967.2 event transfers stress farther west covering the Izmit Gulf area which has experienced large earthquakes in historical time. Clear aftershock activity was associated with the 1967.2 and 1967.1 events (solid circles).

Plate 6. Coulomb stress change due to the previous earthquakes plus these in 1968 and 1969. The 1968 earthquake increases stress on the 1981.1 fault; it decreases it on the 1981.2 and 1983 faults. The background seismicity (open circles) is plotted between the 1969 and 1970 for the events in western Turkey, between the 1968 and 1975 for the events in the Gulf of Saros, between the 1968 and 1978 for the events in the northwest part of the Aegean and between the 1968 and 1981.1 for the events in the southern part of the Aegean (see Figure 4). The major part of the seismicity occurred in Coulomb stress increase areas. The aftershock activity associated with all these shocks is plotted with solid circles.

Plate 7. Coulomb stress change due to the previous earthquakes plus those in 1970, 1975, 1978 and 1981.1. The 1981.1 earthquake triggered the 1981.2 event which occurred 8 days later. The background seismicity (open circles) is plotted between 1970 and 1981.2 for the events in western Turkey, between the 1975 and 1981.2 for the events in the Gulf of Saros, between the 1978 and 1981.2 for the events in the northwest part of the Aegean and between the 1981.1 and 1981.2 for the southern part of the Aegean (see Figure 4). The aftershock activity associated with all these shocks is plotted with solid circles.

Plate 8. Coulomb stress change due to the previous earthquakes plus those in 1981.2 and the 1982. This last shock adds load on the nearby 1983 fault which was previously in a stress shadow. The background seismicity (open circles) that occurred between the 1981.2 and 1983 events is shown with the 1982 and 1981 aftershocks (solid circles).

Plate 9. Coulomb stress change due to all the events with the seismicity between 1983 and 1996 superimposed. A reasonable correlation between background seismicity (open circles) and enhanced Coulomb stress is found (see text) except near the borders of the region which are influenced by earthquakes not modeled in this study (see Figure 5).

Plate 10. Coulomb stress change including all the events since 1912 and active faults in the area. By comparing areas of increased Coulomb stress and active faults, likely candidate faults for future events can be identified.

In Plate 3 we add the effects of the 1944.2, 1944.3, 1953 and 1956 events. The 1956 earthquake seems to have little influence on subsequent events. The 1953 event loads the 1964 fault by 0.1-2.0 $\times 10^5$ Pa. Although they are not well located, aftershocks occur near to this fault plane. The 1944.2 event increases the load on the fault segments that will rupture in 1970 by up to 0.1×10^5 Pa.

In Plate 4 we add the 1957, 1963, 1964 and 1965 earthquake ruptures. Movement on the 1957 fault adds a further load (up to 3.0×10^5 Pa) on the 1967.2 fault zone. The aftershock sequence falls in the red lobe induced by the 1943 and 1957 events. The 1965 earthquake increases the stress on the 1967.1 fault by less than 0.1×10^5 Pa. Its early aftershocks were located near the fault plane and then appear to have migrated to the southwest into an area of decreased Coulomb stress. However, this included four events of magnitude > 5. We lack sufficient information to model these events, and the static stress change associated with them could have modified the stress distribution due to the main shock sufficiently to explain their distribution.

In Plate 5 the 1967.1 rupture in the Aegean Sea loads the 1968 fault zone by up to 3.0×10^5 Pa and the fault that will rupture in 1981.1 by a modest 0.1×10^5 Pa. With one exception all the aftershocks occurred within the 0.1×10^5 Pa contour with a concentration near the future 1968 epicenter. The 1967.2 event also occurred releasing the load on the eastern part of the North Anatolian Fault induced by the

1943, 1944.1 and 1957 earthquakes. Its aftershocks are located near the fault rupture or in a lobe of increased Coulomb stress at its eastern extremity.

In Plate 6 the 1968 and 1969 faults, which were previously loaded by the 1967.1 and 1942 earthquakes, respectively, moved. The 1968 event increases the stress loading by 1.0×10^5 Pa on the northeast extremity of the 1981.1 fault and by 0.2×10^5 Pa on the southwest extremity of the 1982 fault. The 1968 aftershocks are located near the center of the fault and in the northeastern lobe of increased Coulomb stress. This event also has the interesting effect of placing the faults that will rupture in 1981.2 and 1983 in regions of reduced Coulomb stress. These reductions, however, are to be more than compensated for by later increases due to the 1981.1 and 1982 events. The 1969 aftershocks are not clearly associated with red lobes. However, the main event and hence the region affected by stress changes is small, and the aftershock location errors are comparable to the dimensions of the stress pattern.

In Plate 7 slip due to the 1970, 1975, 1978 and 1981.1 earthquakes is added. All these earthquakes were located in areas of Coulomb stress increase due to the 1944.2, 1912, 1932 and 1968 earthquakes. The 1981.1 earthquake raised stress by up to 2.0×10^5 Pa on the 1981.2 fault. The aftershocks that occurred between the 1981.1 and the 1981.2 events are located close to the main rupture and at both its extremities. We observed a similar pattern for the 1970 aftershocks. Most of the 1975 aftershocks are located in the red lobe created by the 1912 and the 1975 ruptures.

Ruptures due to the 1981.2 and 1982 earthquakes are included in Plate 8. The 1981.2 extended the rupture zone of the 1981.1 event to the southwest, and the aftershock zone due to both events is apparently enlarged both to the southwest and to the northeast. Those aftershocks, which cannot be assumed to be closely related to the main rupture system, almost all fall within the red lobes associated with the 1981.1 and 1981.2 events. The 1982 earthquake raises the stress by up to 2.0×10^5 Pa on the 1983 fault. Its aftershock zone appears to be limited to the west by the de-stressed area due to the 1932 event, and only a very few events are situated near the fault which will move in 1983. However, before the 1983 event the background seismicity increases in the whole area.

In summary, we observe a clear correlation between regions of increased Coulomb stress and the location of 16 out of 29 events (1935, 1939, 1944.1, 1953, 1957, 1964, 1967.2, 1968, 1969, 1970, 1975, 1978, 1981.1, 1981.2, 1982, 1983). This is based on the assumption that a clear correlation only occurs when Coulomb stress is increased by more than 0.1×10^5 Pa. The 1942 event might have been in a region of such increased stress, but the information available to us does not permit us to be certain. The time interval between the Coulomb stress change and the subsequent events varies from 8 days to 63 years with a mean of 18 years. All the 10 events of magnitude > 6 that occurred after 1967 are located in areas of Coulomb stress increase; only the earlier events are not. The latter could, however, have been in areas of Coulomb stress increase resulting from the rupture of yet earlier earthquakes. The 1912, 1943, 1944.3 and 1963 events could be related to events in 1873, 1859, 1809 in the Gulf of Saros, to the 1889 earthquake in the Edremit Gulf and to the 1894 earthquake in the Izmit Bay, respectively [*Ambraseys and Finkel*, 1991]. Preliminary modeling of these events (Figure 5) shows that the 1912, 1943, 1944.3 and 1963 events fall entirely or partly in areas of Coulomb stress increase (> 0.1×10^5 Pa). We have made no attempt to model these relations better in this study. We do not, as yet, know historical events to explain the events in 1919, 1924, 1928, 1932, 1944.2, 1956, 1965 and 1967.1, but they may be found in the future. The 1928 and 1944.2 events occurred in areas with a positive static stress increase induced by the 1924 event and the 1967.1 event occurred in a region where stress was increased by the 1965 event. The increases are lower than 0.1×10^5 Pa that we have taken as a threshold, but may nonetheless be significant.

8. Coulomb Stress Change and Background Seismicity

After 1967 there was an improvement in the seismic network covering parts of the region we study and it is possible to estimate numerically the correlation between the background seismicity and Coulomb stress change (Plates 6, 7, 8 and 9). To avoid the confusion due to many events close to a fault plane, we exclude aftershocks and look only at background seismicity. In Plate 6 there is a clear correlation between the seismicity and the Coulomb stress increase due to the earthquakes modeled up to 1969. There is enhanced seismic activity in the area of the 1975 and 1978 shocks and in the increased Coulomb stress region due to the 1968 and 1967.1 earthquakes. There are many shocks in the destressed area associated with the 1965 and 1932 events. However, more than 45% of the 863 events, and 9 out of 10 events with M_s>5.0, occurred in areas of Coulomb stress increase (> 0.1×10^5 Pa). More than 30% of

the events occurred in areas where Coulomb stress was increased by more than 0.3×10^5 Pa, while only 21% of the events (and no events with M_s>5) occurred in areas of Coulomb stress decrease ($< -0.3 \times 10^5$ Pa). Only 10% of the events occurred in the areas where the Coulomb stress decrease was more than 1.0×10^5 Pa.

Plate 7 shows the static stress changes resulting from modeling earthquakes between 1912 and 1981.1. There is a clear increase in seismicity in western Turkey after the 1970 Gediz earthquake while the seismic activity previously located in the region of Coulomb stress increase due to the 1968 earthquake is shut down by the 1981.1 earthquake. More than 50% of the 941 events occurred in areas of Coulomb stress increase ($> 0.1 \times 10^5$ Pa) and 41% in areas of Coulomb stress increase of more than 0.3×10^5 Pa. Less than 35% of the events occurred in areas of Coulomb stress decrease and less than 15% where the Coulomb stress was decreased by more than 1.0×10^5 Pa.

In Plate 8 clusters can be seen in the seismicity. The clusters north of the 1953 event and south of the 1969 and 1942 events are located in areas of Coulomb stress increase. However, others, northeast of the 1964 event or in the north Aegean trough, are not. More than 40% of the 368 events occurred in areas of Coulomb stress increase and 31% occurred in areas of Coulomb stress increase greater than 0.3×10^5 Pa. Nearly 40% of the events, however, occurred in areas of Coulomb stress decrease, but < 12% occurred where the Coulomb stress was decreased by more than 1.0×10^5 Pa.

In Plate 9 we show the present static stress change due to all of the 29 major earthquakes in the area including the 1983 event. We can compare it with all the subsequent $M \geq 3$ events in the catalogue. In the north Aegean Sea the 1983 aftershocks are prominent. However, the continuing seismicity in this area still shows trends associated with the 1982-1983 ruptures (the northern branch of the North Anatolian Fault). Less continuous trends occur along the 1968 and 1981.1-1981.2 ruptures associated with the southern branch of the North Anatolian Fault. There are two other trends associated with strike-slip faulting on the northern branch of the North Anatolian Fault, one west of the 1967.2 rupture and the second east of the 1912 event in the western part of the Sea of Marmara. There are also clusters of seismicity more or less delimited by the areas of Coulomb stress increase. For example, one cluster is associated with the 1975 event, two others are enclosed by the Coulomb increases due to 1939, 1919, 1969 and 1953 events and by the 1964, 1969 and 1970 events. Nearly 55% of the 5890 events have occurred in areas of Coulomb stress increase, and 42% occurred in areas where Coulomb stress was increased by more than 0.3×10^5 Pa. Less than 35% of the events occurred in areas of Coulomb stress decrease, and only 15% where the Coulomb stress decreased by more than 1.0×10^5 Pa.

Taking all of the plates together, more than 31% of the background seismicity occurred in the areas where Coulomb stress was increased by more than 0.3×10^5 Pa, and < 15% occurred in the Coulomb stress shadows where the stress decreased by more than 1.0×10^5 Pa. It is perhaps more useful to look at the density of earthquakes in areas of Coulomb stress increase and decrease (Table 3). Where the Coulomb stress increase is greater than 0.3×10^5 Pa, we find more than 4 times the number of events per unit area than regions where Coulomb stress is decreased by more than 1.0×10^5 Pa.

9. Discussion

The region we have studied is a large and fast deforming zone with widespread seismicity on a variety of faults with different mechanisms that transfer the strike-slip motion from Turkey to the extensional Aegean regime. From the beginning of the century there have been 29 earthquakes with $M_s \geq 6.0$ that have been used here to calculate the Coulomb stress field resulting from their rupture. Out of the 29 events, 16 are clearly related to Coulomb stress increased due to previous earthquakes, and all of the last 10 events fall into this category. We have good grounds for believing that four others are related to earlier historical earthquakes. Three other events are located in areas of Coulomb stress increase, but the increase is less than 0.1×10^5 Pa. Thus the observation that 16 out of 29 events are related to regions of stress increase is robust, with some evidence that 23 out of 29 were also related to stress increases. The remaining events may be related to Coulomb stress increases, but if we want to have a clearer picture of the relations, we need to know the location and the mechanism of all the historical earthquakes that have occurred in the area since 1800 and study Coulomb stress interaction over a longer time period. This information is now being assembled.

The background seismicity fits with the areas of Coulomb stress increase, although events apparently occur in Coulomb stress shadows. This need not be a real effect for a number of reasons. The poor

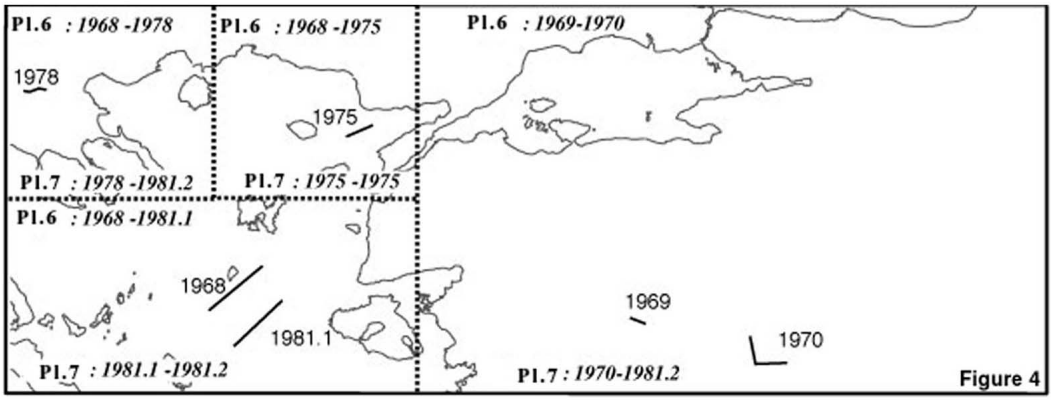

Temporal and spatial windows of background seismicity used in Plates 6 and 7.

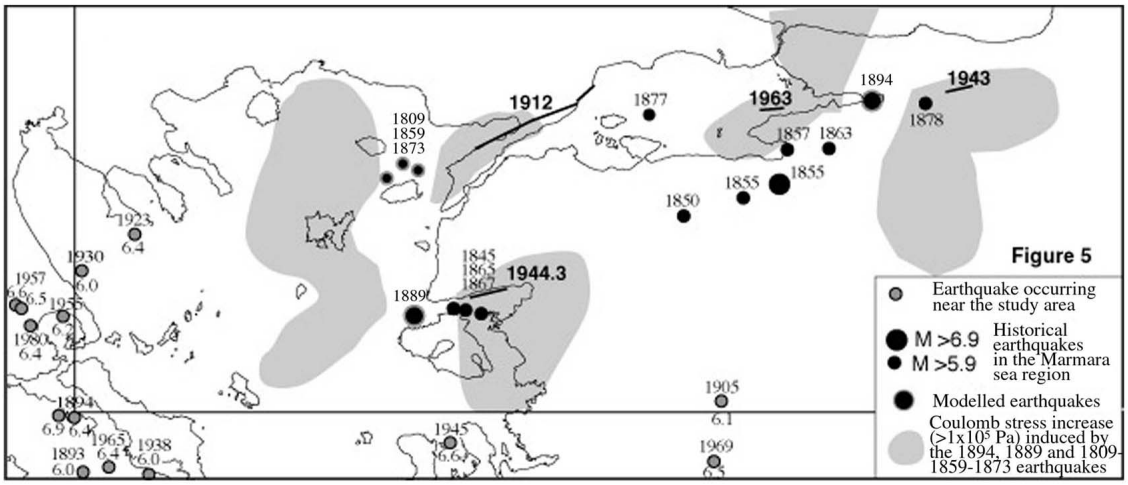

Historical events and events near the edge of the studied area [Ambraseys, 1988; Ambraseys and Jackson, 1990; Ambraseys and Finkel, 1991] which could influence the Coulomb stress change and the background activity. Regions that were probably increased in stress by some of these events are shown by shading.

epicentral locations discussed earlier is one, but other effects may be important. For events relatively close to the faults that have slipped, this could be related to the geometry and the slip distribution of the fault rupture which we cannot define precisely for many of the shocks in this study. Near the edges of the study area, major events outside could have influenced the stress distribution inside. Such events [*Ambraseys and Jackson*, 1990; *Ambraseys*, 1988] near the edge of the study area are shown in Figure 5 and will modify the Coulomb stress pattern in the SW part of the Aegean Sea and south of the Lesvos Island. A further reason for the seismicity not correlating with the Coulomb stress is that within a horizontal distance of one or two fault depths (25 km) stress patterns vary with depth for dip-slip faults. Here we only consider the stress changes at the midseismogenic depth (6.5 km). Finally, we have no clear idea of the stress loading mechanism for dip-slip faulting. Many authors believe that nearly vertical strike-slip faults are loaded from below by a creeping continuation of a fault with the same (or similar) geometry at depth to that nearer the surface [e.g., *Stein et al.*, 1997; *Deng and Sykes*, 1997]. However, it is popular to consider that the seismogenic zone for dip-slip faulting regions is marked by a transition to a viscoelastic lower crust [*King et al.*, 1988; *Stein et al.*, 1988; *Ellis and King*, 1990; *Kusznir et al.*, 1991; *Burov and Diament*, 1992; *Armijo et al.*, 1996]. Whether or not this is correct, it is clear that dip-slip faults cannot simply continue with constant dip to depth. Thus lower crustal processes may be expected to produce stresses in the seismogenic zone that we do not yet know how to model.

A better picture of stress accumulation would include such secular loading including boundary forces or continuous slip on features in the lower crust, but because of the complications just outlined, it is certainly beyond the scope of this paper. Nonetheless, it is clear that even without understanding the loading processes, if future major events behave in a similar way to those over the last 75 years, then regions of reduced Coulomb stress are less likely to be potential sites for future events, and disastrous events are more likely to occur in the limited "red" regions where Coulomb stress has been increased (Plate 10).

10. Conclusions

The stress interactions of 29 earthquakes ($M_s \geq 6$) that have occurred since 1912 on and around segments of North Anatolian fault in the Sea of Marmara region and North Aegean have been investigated by using Coulomb failure criterion. If we consider that interaction occurs only when an event occurs in a region where the stress has been increased by 0.1×10^5 Pa or more, then 16 events are unambiguously related to earlier events. A further four events were almost certainly related to earlier events for which we have less information. If we are prepared to consider that events can be related to increases of Coulomb stress of less than 0.1×10^5 Pa, then a further three events could be included. Of the remaining six events none occurred in a Coulomb shadow, and in the future, information will be forthcoming about historical events that may explain their locations; all occur at the beginning of the time period that we consider. Our modeling does not include tectonic loading, and this may also help explain the distribution of these events. It is also striking that in some cases, faults that have been placed in a stress shadow by earlier events are reloaded soon before they slip by motion on adjacent faults. We consider the relation of aftershocks and background seismicity to Coulomb stress changes. While limitations of data quality and modeling method limit our ability to make robust comparisons, clear correlations can be observed.

From this study and others over the last few years, it has become clear that changes in Coulomb stress are associated with regions where future damaging earthquakes are likely to occur. Thus even if the correlation between regions of enhanced Coulomb stress and future events is less close than we appear to observe, regions of increased stress must be regarded as subject to greater hazard than elsewhere. In the Turkish and Aegean region that places at substantial risk 20% of the total area that we have studied. Major events do not appear to occur in regions of reduced Coulomb stress, and thus the 50% of the region can be considered to have lower seismic risk. This should be treated with caution, however, since we have seen that a region can be loaded and then subject to an earthquake soon afterward.

By extending Coulomb modeling to include events from historical data and those deduced from tectonic studies we may expect to narrow even further the areas of hazard. By combining the stress change map with the map of active faulting (Plate 10), likely locations for the occurrence of future earthquakes can be refined. Faults in the Izmit Bay area, the western part of Biga peninsula, the Saroz Gulf and a part of western Sea of Marmara must be regarded as posing a specific hazard.

While we make no attempt in this study to suggest the time when future events may occur, their likely occurrence will be decades rather than centuries in the future. Thus particular attention should be paid to

hazard mitigation measures in areas of increased Coulomb stress.

Tables:

Table 1. Modeled Fault Coordinates

Earth-quakes	Segments	Epicentral Coordinates in UTM, km				Slip, m		Dip, deg
		X Start	Y Start	X End	Y End	Shear	Dip	
1912	3	453	4476	484	4491	2.00	0.00	90
		484	4491	524	4508	3.90	0.70	90
		524	4508	536	4519	2.20	1.25	90
1919	2	537	4329	545	4335	0	-1.60	45
		545	4335	554	4353	1.10	-1.10	45
1924	1	726	4333	772	4331	0	-0.20	45
1928	1	710	4354	717	4343	0	-0.35	45
1932	2	242	4490	232	4491	0	-2.00	45
		232	4490	218.	4494	0	-2.00	45
1935	1	538	4558	558	4503	0	-0.85	45
1939	1	502	4317	517	4324	0	-0.75	45
1942	1	587	4347	598	4342	0	-0.35	45
1943	1	795	4520	811	4522	0.75	0	90
1944.1	4	878	4512	891	4515	3.50	-1.00	90
		891	4515	914	4525	3.50	-1.00	90
		914	4525	979	4540	2.00	-2.00	90
		979	4540	1050	4550	1.50	-0.50	90
1944.2	1	703	4324	706	4318	0	-0.28	45
1944.3	1	473	4378	448	4371	1.10	-1.10	60
1953	4	563	4435	555	4437	2.00	0	90
		555	4437	542	4428	3.50	0	90
		542	4428	526	4419	3.50	0	90
		526	4419	509	4416	2.00	0	90
1956	1	761	4412	777	4411	0	-0.35	45
1957	2	839	4499	849	4501	2.50	0	90
		849	4501	876	4510	2.50	0	90
1963	1	661	4506	667	4507	0	-0.65	60
1964	1	586	4439	625	4431	0	-1.20	45
1965	1	225	4353	236	4363	0	-0.68	45
1967.1	1	280	4350	292	4338	0	-0.68	45
1967.2	5	780	4504	798	4504	0.70	-0.70	60
		798	4504	808	4500	1.50	-1.50	60
		808	4500	827	4498	2.00	-1.00	60
		827	4498	843	4500	2.50	0	90
		843	4500	857	4503	2.50	0	90
1968	1	307	4342	348	4385	3.20	0	90
1969	1	630	4341	617	4345	0	-0.35	45
1970	4	707	4333	729	4333	0	-2.40	15
		700	4331	702	4323	0	-1.60	35
		701	4322	707	4315	0	-1.60	35
		707	4315	729	4315	0	-2.40	35
1975	1	427	4480	412	4473	0.67	-0.67	60
1978	3	178	4505	182	4504	0	-0.70	45
		182	4504	191	4504	0.30	-0.60	45
		191	4504	194	4507	0	-0.70	45
1981.1	1	325	4321	370	4362	3.20	0	90
1981.2	1	314	4303	327	4314	0.75	0	90
1982	1	270	4408	294	4428	2.25	-0.17	90
1983	1	296	4430	324	4444	2.25	0.00	90

Ellipsoid WGS-84, zone 35, coordinates in Universal Transverse Mercator (UTM). All faults extend from surface to 12.5 km depth. Positive shear slip for right-lateral and positive dip slip for reverse movement

Table 2. Locations, Magnitudes, and Focal Mechanisms of the Modeled Earthquakes

No.	Date	Epicenter °N	Epicenter °E	M_s	Depth, km	Azim, deg	Dip, deg	Rake, deg	Quality
1	Jan. 19, 1912	40.75	26.90	7.4		68	55	-145	B
2	Nov. 18, 1919	39.10	27.40	6.9					F
3	Nov. 20, 1920	39.08	30.14	6.0					F
4	May 2, 1928	39.41	29.54	6.2					F
5	Sept. 26, 1932	40.50	23.90	7.0					B
6	Feb. 4, 1935	40.70	27.60	6.4		100	40	-90	E
7	Sept. 22,1939	39.05	26.93	6.5					E
8	Nov. 15, 1942	39.38	28.08	6.2					E
9	June 20, 1943	40.80	30.40	6.4					C
10	Feb. 1, 1944	41.50	32.40	7.3					A
11	June 25, 1944	39.03	29.37	6.0					B
12	Oct. 6, 1944	39.70	26.80	6.8		262	41	-70	E
13	March 18, 1953	40.00	27.40	7.2		60	90	180	A
14	Feb. 20, 1956	39.86	30.49	6.4	9	140	56	309	C
15	May 26, 1957	40.67	30.86	7.0					A
16	Sept. 18, 1963	40.90	29.20	6.4	15	340	56	-82	D
17	Oct. 6, 1964	40.30	28.23	6.9	14	100	40	-90	C
18	March 9, 1965	39.34	23.82	6.3	7	135	85	15	D
19	April 3, 1967	39.25	24.60	6.5	12	313	43	-56	D
20	July 22, 1967	40.67	30.69	7.1	12	275	88	-178	A
21	Feb. 19, 1968	39.40	24.94	7.2	15	311	90	20	D
22	March 23, 1969	39.14	28.48	6.0	8	112	34	-90	C
23	March 28, 1970	39.21	29.51	7.2	8	308	35	-90	A
24	March 27, 1975	40.42	26.14	6.6	7	68	55	-145	D
25	June 20, 1978	40.78	23.24	6.4	7	271	42	-74	A
26	Dec. 19, 1981	39.22	25.25	7.2	10	60	79	175	D
27	Dec. 27, 1981	38.91	24.92	6.4	6	216	79	175	D
28	Jan. 18, 1982	39.96	24.39	6.9	7	233	62	187	D
29	Aug. 6, 1983	40.14	24.74	6.9	7	47	83	180	D

Table 3. Number of Earthquakes (events) in Plates 7-9 and Figure 4 averaged by the area of increase ($> 0.1 \times 10^5$ and $> 0.3 \times 10^5$ Pa) and decrease of Coulomb stress ($< -1.0 \times 10^5$ Pa and $< -0.1 \times 10^5$ Pa). Note that Figure 4 shows the regions and time periods only. The Coulomb changes, though calculated and used to create this table, are not reproduced.

	$< -1 \times 10^5$ Pa	$< -0.1 \times 10^5$ Pa	$> 0.1 \times 10^5$ Pa	$> 0.3 \times 10^5$ Pa
Plate 7	0.01	0.01	0.043	0.046
Plate 8	0.015	0.018	0.05	0.07
Figure 4	0.0048	0.0075	0.020	0.021
Plate 9	0.09	0.095	0.37	0.41

In events/km^2

Appendix: Earthquakes Used in the Modeling

In this account, fault lengths and slip amplitudes are often derived or checked using the relations published by *Kanamori and Anderson* [1975]. Where this has been done, we simplify the reference to "using KA."

A1. August 9, 1912, Murefte Sarkoy Earthquake, M_s=7.4; Q=B

The first earthquake that we have modeled occurred in southeast Thrace between the Gulf of Saros and the Sea of Marmara. It was followed by several large aftershocks (August 10, 1912, M_s = 6.3; September 13, 1912, M_s = 6.9; September 27, 1912, M_s = 6.6 [*Ambraseys and Finkel*, 1987]) to the west of the main shock. Reports and photographs taken just after the earthquake are available [*Macovei*, 1912; *Mihailovic*, 1927, 1933]. *Ates* [1982] maps the ground deformation which occurred on the 50 km long strike-slip fault linking the Marmara and the Saros fault systems [*Ates and Tabban*, 1976; *Öztin*, 1987; *Barka*, 1992; *Ambraseys and Finkel*, 1987]. The surface rupture pattern was complex with a substantial right-lateral strike-slip component (up to 3 m) [*Ambraseys and Finkel*, 1987]. In this area, the northern branch of the North Anatolian fault steps from the Sea of Marmara to the Aegean Sea such that it should locally have a reverse component. This hypothesis is supported by the microseismicity, by the kinematic model based on GPS data developed by *Straub* [1996] and by the long-term morphology of the area associated with young folding and uplift [*Yaltirak*, 1996]. The eastern part of the fault appears as a

positive flower structure so although there is clear evidence of contraction there is no obvious preferred dip direction. We model the reverse component of the rupture in this area as a closure vector normal to a vertical fault plane. We extend the rupture seen on land by 15 km to the east and 25 km to the west to fit the IX isoseismal line (giving L = 90 km) and a mean displacement compatible with the observed strike-slip component (using KA). We define three fault segments with a vertical dip: the eastern one and middle ones have a reverse component, while the western one, bounding the Gulf of Saros, is pure strike-slip.

A2. November 18, 1919, Soma Earthquake; M_s=6.9; Q=F

The Soma earthquake occurred south of the North Anatolian fault in western Anatolia between the towns of Soma, Bergama and Balikesir [*Pinar and Lahn*, 1952; *Ambraseys*, 1988]. Detailed information is not available for this event due to the unsettled situation in the country at that time [*Ambraseys*, 1988]. However, it occurred at the eastern extremity of the Bakircay normal fault zone which also ruptured during the 1939 earthquake. Examining Landsat images and the topographic maps together with macroseismic information and the faults mapped in the area, we were not able to clearly associate it with one fault. As east-west normal faulting and right-lateral strike-slip faulting are found in the area, we model this event as resulting from a 30 km long, right-lateral, normal fault dipping to the north (like the nearby 1939 earthquake) in the area where ground rupture were reported. We assume a dip of 45° and a mean displacement of 1.4 m (using KA).

A3. November 20, 1924, Altintas Earthquake; M_s=6.0; Q=F

Not much is known about this earthquake which occurred in western Anatolia [*Ambraseys*, 1988], east of the 1970 Gediz earthquake. In this area, east-west normal faulting is dominant and was associated with the 1956 Eskisehir and the 1970 Gediz earthquakes. We were not able to associate this event with a specific fault. We assume that the event occurred on a east-west, normal fault located near the epicenter with a dip of 45° which is compatible with the known tectonics of the area. A 10 km fault length and a mean displacement of 0.2 m was calculated using KA.

A4. May 2, 1928, Emet Earthquake; M_s=6.2; Q=F

This event occurred in the Kocasu valley in a similar tectonic environment to the Altintas earthquake [*Ambraseys*, 1988] and 50 km north of the Gediz fault system. In this area, NNW-SSE striking normal faults dipping to the ENE were reactivated during the earthquakes in 1970 and 1944. We model the event with a 12.5 km long normal fault rupture with a mean displacement of 0.35 m (using KA) and a dip of 45°. The strike is taken to be the same as the $M \geq 6$ events that have occurred in the same area.

A5. September 26, 1932, Ierissos-Chalkidiki Earthquake; M_s=7.0; Q=B

This event occurred in northern Greece, in the southeastern part of the Chalkidiki peninsula north of the North Aegean Trough and was followed by strong aftershocks (September 26,1932, M_s = 6.0; September 29, 1932, M_s = 6.2; May 11, 1933, M_s = 6.3). It reactivated an east-west striking, south dipping, normal fault over at least 15 km on land [*Floras*, 1933; *Maravelakis*, 1933; *Georgalas and Galanopoulos*, 1953; *Pavlides and Tranos*, 1991] with normal displacements up to 2 m (down to the south). The morphological trace of the fault continues seaward forming a peninsula and since a small tsunami and coastal deformation occurred, we suggest that the fault rupture could have extended seaward for about 10 km. This is compatible with the magnitude of the earthquake . We choose to model this event as a 25 km long normal fault with a dip of 45° and a mean displacement of 2 m.

A6. January 4, 1935, Marmara Earthquake; M_s=6.4; Q=E

Two earthquakes of nearly equal magnitude, spaced 2 hours apart occurred on the southwest extremity of the Sea of Marmara, north of the Marmara Islands. The isoseismal map [*Ambraseys*, 1988] places the event near to the east-west, north dipping, normal fault system forming the southern edge of the Sea of Marmara [*Barka*, 1992; *Wong et al.*, 1995]. A spring dried up on Marmara Island as may be expected in the footwall of a normal fault [*Muir-Wood and King*, 1993]. As the two events cannot be separated, we model them as resulting from one single rupture (equivalent M_s=6.6) on the fault system north of the Marmara Island (east-west striking normal faulting dipping to north). We adopt a dip of 45° and, using KA, take the fault to have a length of 20 km and to have slipped 0.85 m.

A7. September 22, 1939, Bergama Earthquake; M_s=6.5; Q=E

The Bergama earthquake occurred near the coast in western Anatolia south of the Edremit Gulf. The isoseismic map [*Eyidogan et al.*, 1991] locates the event at the western extremity of the Bakircay normal fault zone [*Arpat and Bingöl*, 1969; *Westaway*, 1990] formed by east-west normal faults dipping to the north. The (poorly constrained) focal mechanism derived by *Ritsema* [1974] indicates east-west normal faulting. We model the rupture to dip at 45° and using KA to be 17 km long with and a mean normal displacement of 0.75 m.

A8. November 15, 1942, Bigadic Earthquake; M_s=6.2; Q=E

The Bigadic earthquake occurred in western Anatolia, south of Balikesir. The villages destroyed were concentrated at the southwest extremity of the Simav normal fault zone [*Ambraseys*, 1988]. In this area, normal faults strike east-west and dip toward the north [*Westaway*, 1990]. We model the rupture as a 12.5 km long normal fault similar to faults mapped and assume a dip of 45° and a mean displacement of 0.35 m (using KA).

A9. June 20, 1943, Hendek-Adapazari Earthquake; M_s=6.4; Q=C

The Hendek-Adapazari earthquake was located east of the Sea of Marmara in the Mudurnu valley, 15 km north of the 1967 rupture. The isoseismal map shows an elongated pattern in the nearly flat plain [*Pamir et al.*, 1943]. The focal mechanism based on *P* wave polarities [*McKenzie*, 1972] indicates almost pure strike-slip motion parallel to the North Anatolian fault. The earthquake probably occurred on a secondary strike-slip fault north of the North Anatolian fault. Using KA, we model the event as a 16 km long right-lateral fault with 0.75 m of displacement.

A10. February 1, 1944 (1944.1), Bolu-Gerede Earthquake; M_s=7.3; Q=A

The Bolu-Gerede earthquake occurred on the North Anatolian fault at the eastern extremity of the studied area. It is the fourth event of the sequence that ruptured the North Anatolian fault from eastern Turkey to the Sea of Marmara [*Ambraseys*, 1970; *Stein et al.*, 1997]. The 1944 surface rupture was mapped over 165 km with a right-lateral slip distribution that reaches 3.5 m to the west and decreases to 1.5 in the east [*Ketin*, 1969; *Ambraseys*, 1970, 1988]. The slip distribution was compiled by *Barka* [1996]. We model it as a 165 km long right-lateral strike-slip fault with the above slip distribution.

A11. June 24, 1944 (1944.2), Saphane Earthquake; M_s=6.0; Q=B

The Saphane earthquake occurred in western Anatolia, southwest of Gediz. The fault rupture reactivated part of a NNW-SSE normal fault system [*Ambraseys and Tchalenko*, 1972] which also ruptured during the 1970 Gediz earthquake. We model it as a NNW-SSE normal fault dipping 45° to the ENE with a fault length of 10 km and a mean displacement of 0.20 m calculated using KA.

A12. October 6, 1944 (1944.3), Ayvacik Earthquake; M_s=6.8; Q=E

The Ayvacik earthquake occurred near the Edremit Gulf and caused heavy damage to Ayvacik and villages on the coast [*Ambraseys*, 1988]. In this area the southern branch of the North Anatolian fault reaches the Aegean Sea through the Edremit Gulf. The earthquake may reactivate one of its segments with mixed strike-slip and normal faulting in the Edremit Gulf. The poorly constrained focal mechanism [*Ritsema*, 1974] indicates nearly pure strike-slip. However, it could have a normal component like the 1975 earthquake in the Gulf of Saros where the northern branch of the North Anatolian fault reaches the Aegean Sea. We choose to model the 1944.3 earthquake to be like the 1975 with an oblique slip on a 60° south dipping fault. The length (25 km) and displacement (1.6 m) were estimated using KA.

A13. March 18, 1953, Yenice-Gönen Earthquake; M_s=7.2; Q=A

The Yenice-Gönen earthquake occurred between the Sea of Marmara to the north and the Edremit Gulf to the south and ruptured the southern branch of the North Anatolian fault over 60 km [*Pinar*, 1953; *Ambraseys*, 1970]. The focal mechanism [*McKenzie*, 1972] indicates pure southwest-northeast right-lateral strike-slip faulting. The slip reaches 3.5 m in the eastern part and drops to 1.5 m at both ends [*Ambraseys*, 1970; *Ketin and Roesli*, 1953; *Roesli*, 1953]. We model the earthquake using the observed

slip distribution and the geometry (length 60 km) of the mapped surface rupture.

A14. February 20, 1956, Eskisehir Earthquake; M_s=6.1; Q=C

The Eskisehir earthquake occurred in western Anatolia, 30 km west of Eskisehir and 100 km north of Gediz [*Ambraseys*, 1988]. The isoseismal map [*Öcal*, 1959a; *Ergin et al*., 1967] indicates that it was on the Eskisehir normal fault system. The focal mechanism [*McKenzie*, 1972] indicates east-west normal faulting. The predominant fault dips toward the north, so we model this event as resulting from the rupture of an east-west normal fault dipping to the north with an angle of 45°. We use KA to calculate a fault length of 11 km and a displacement of 0.30 m.

A15. May 20, 1957, Abant Earthquake; M_s=7.0; Q=A

The Abant event occurred on the North Anatolian fault at the eastern side of our study area. It is the fifth event of the North Anatolian fault sequence [*Barka*, 1996; *Stein et al.*, 1997]. The 40 km long surface rupture which started where the 1944.1 rupture ended, was mapped by *Ambraseys* [1970, 1988]. The focal mechanism [*McKenzie*, 1972] indicates strike-slip faulting. The slip [*Öcal*, 1959b] unfortunately is not well constrained being measured at only two localities (1.4 and 1.6 m). Using KA we model the event to have been due to an average of 2.5 m of strike-slip motion on a 40 km stretch of fault.

A16. October 18, 1963, Yalova Earthquake; M_s=6.4; Q=D

The Yalova earthquake occurred in the southeast Sea of Marmara, just north of the Yalova peninsula. It has a reliable focal mechanism solution indicating pure northwest-southeast normal faulting [*Taymaz et al*., 1991]. The main damage was localized on the southern coast of Sea of Marmara so it seems to have reactivated one segment of the northeast dipping normal fault system forming the southern edge of the peninsula [*Barka and Kadinsky-Cade*, 1988; *Wong et al*., 1995] and not the fault plane dipping toward the south as proposed by *Taymaz et al*. [1991]. We model the event as a normal fault dipping northward with a dip of 60°, a length of 16 km and displacement of 0.60 m using KA.

A17. October 6, 1964, Manyas Earthquake; M_s=6.9; Q=C

The Manyas earthquake occurred on land south of the Sea of Marmara between the Manyas lake and the Ulubat lake on the southern branch of the North Anatolian Fault. The focal mechanism solution [*Öcal et al*., 1968; *Taymaz et al*., 1991] indicates east-west normal faulting. The 40 km long complex surface faulting (en echelon ground rupture and fissuring over a wide zone) was interpreted as resulting from right-lateral strike-slip motion [*Erentöz and Kurtman*, 1965; *Ketin*, 1966]. However, the field evidence is not very clear, whereas the focal mechanism is, so we choose to model the event as a 40 km long east-west normal fault dipping to the north with a dip of 45° and a mean displacement of 1.2 m (using KA).

A18. March 9, 1965, Aegean Earthquake; M_s=6.3; Q=D

This event occurred in the Aegean Sea at the southwest extremity of the North Aegean Trough. The focal mechanism indicates right-lateral strike-slip faulting on a northeast-southwest plane [*Taymaz et al*., 1991]. In this area a major fault system, the northern branch of the North Anatolian fault, limits the southwestern edge of the North Aegean Trough. So we model this event as a northeast-southwest striking, right-lateral fault with a length of 14 km and a slip of 0.60 m (using KA).

A19. March 4, 1967 (1967.1), Aegean Earthquake; M_s=6.5; Q=D

This event occurred in the Aegean Sea at the northwest extremity of the Skyros Basin, south of the North Aegean Trough. The predominantly normal faulting focal mechanism [*Taymaz et al.*, 1991] defines two possible fault planes: one striking east-west with a dip toward the south, the other northwest-southeast with a dip toward the northeast. The major normal faults in the area bounding the western edge of Skyros Basin are oriented like the second nodal plane. So even if this event is located northwest of those faults, we choose to model it like a northwest-southeast normal fault with a dip of 45°, a fault length of 18 km and a displacement of 0.70 m (using KA).

A20. July 22, 1967 (1967.2), Mudurnu Earthquake; M_s=7.1; Q=A

The Mudurnu earthquake occurred east of the Sea of Marmara on the North Anatolian fault and extended toward the west the rupture associated with the 1957 Abant earthquake. It is the most westerly and the last earthquake of the North Anatolian fault sequence [*Barka*, 1996; *Stein et al.*, 1997]. The focal mechanism based on *P* wave polarities [*Canitez*, 1972] and on body wave inversion [*Taymaz et al.*, 1991] indicates pure, east-west, strike-slip faulting. The main shock was located in the eastern part of the rupture zone, and most of the aftershocks were located west of it [*Ambraseys and Zatopek*, 1969]. A large aftershock (July 30, 1967, m_b = 5.6) occurred at its western extremity with a pure normal fault mechanism striking northwest-southeast [*Stewart and Kanamori*, 1978; *Jackson and McKenzie*, 1984]. It illustrates the change that occurs on the North Anatolian fault in this area between pure localized strike-slip motion to the east and more distributed oblique (normal and strike-slip) motion on several branches to the west. For the modeling, we use the detailed maps of the 80 km long surface rupture and the fault slip distribution [*Ambraseys et al.*, 1968; *Ambraseys and Zatopek*, 1969; *Güçlü*, 1969] which is greatest (2.5 m) in the east and decreases steadily to the west.

A21. February 19, 1968, Agios Efstratios Earthquake; M_s=7.2; Q=D

The Agios Efstratios earthquake occurred in the Aegean Sea, south of the Agios Efstratios island on the northern edge of the Skyros Basin [*Pavlides and Tranos*, 1991]. The focal mechanism [*Taymaz et al.*, 1991; *Kiratzi et al.*, 1991] indicated right-lateral strike-slip faulting striking northeast-southwest consistent with the orientation of the southern branch of the North Anatolian fault. The aftershock sequence also defined a northeast-southwest trend [*North*, 1977]. We model the event as a right-lateral strike-slip fault with a length of 60 km (similar to the right-lateral 1953 earthquake of the same magnitude) and a mean displacement of 3.2 m (using KA).

A22. March 22, 1969, Demirci Earthquake; M_s=6.0; Q=C

The Demirci earthquake occurred in western Anatolia in the Simav normal fault system [*Ketin and Abdüsselamoglu*, 1969; *Ambraseys and Tchalenko*, 1972; *Westaway*, 1993]. It was followed by a strong aftershock of nearly equal magnitude (March 25, 1969, M_s=6.0, M_o=1.7 × 10^{18} N m) [*Jackson and Fitch*, 1979]. Using body wave inversion, *Eyidogan and Jackson* [1985] determined a seismic moment of M_o=0.98 × 10^{18} N m. on a WNW-ESE striking normal fault. Either nodal plane could be the fault plane as there was no surface rupture. However, the northern fault dipping toward the south is the dominant in the morphology, and *Eyidogan and Jackson* [1985] concluded that the two shocks were associated with motion on this fault. We therefore model both events as resulting from a single rupture of M_o=2.68 × 10^{18} N m dipping south at 45°, a length of 12.5 km and a displacement of 0.35 m (using KA).

A23. March 28, 1970, Gediz Earthquake; M_s=7.2; Q=A

The Gediz earthquake occurred in western Anatolia, east of the Simav fault system near Gediz. About 40 km of complicated normal faulting trending both to the NNW-SSE and east-west down thrown to the east and north was mapped by *Ambraseys and Tchalenko* [1972]. The aftershock sequence defined a 40 km wide, 200 km long, east-west zone with at least 23 $M \geq 5$ events [*Ambraseys and Tchalenko*, 1972; *Jackson and Fitch*, 1979]. The observed seismograms show considerable complexity and were modeled using three main subevents [*Eyidogan and Jackson*, 1985]. The first subevent occurred on 15 km long NNW-SSE segment with a mean displacement of 1.6 m and a dip of 35°. It then triggers the second subevent which ruptures the 24 km long east-west segment with a mean displacement of 2.4 m and a dip of 35° [*Eyidogan and Jackson*, 1985]. The displacements calculated using the moment of each subevent are consistent with the observed surface slip [*Ambraseys and Tchalenko*, 1972]. All the remaining complexity of seismograms can be explain by slip on a ~15° dipping fault extending the second fault segment from a depth of 12.5 to 17.5 km [*Eyidogan and Jackson*, 1985]. We model this multiple event using these three subevents described.

A24. March 27, 1975, Saros Earthquake; M_s=6.6; Q=D

The Saros earthquake occurred offshore west of the Sea of Marmara in the Gulf of Saros, a pull-apart basin associated with the northern branch of North Anatolian fault. The focal mechanism indicates strike-slip, normal fault, rupture [*Taymaz et al.*, 1991] with the right-lateral plane ENE-WSW consistent the orientation of the North Anatolian fault and with a ~ 60° dip toward southeast. We model the event as an oblique fault with a length of 20 km and displacement of 0.95 m calculated using KA.

A25. June 20, 1978, Thessaloniki Earthquake; M_s=6.4; Q=A

The Thessaloniki earthquake occurred in northern Greece, north of the North Aegean Trough, east of Thessaloniki. *Soufleris and Stewart* [1981] and *Soufleris and King* [1981] derived a seismic moment of 5.2×10^{18} N m and a normal focal mechanism striking east-west. Surface ruptures (mainly open cracks of a few centimetres) were documented on east-west normal fault [*Mercier et al.*, 1979], some at the base of a major normal fault dipping toward the north. The aftershock zone was concentrated north of the main fault rupture, suggesting that the earthquake rupture dipped to the north [*Soufleris et al.*, 1982]. Furthermore, it could be divided in three clusters: east, central and west of the surface rupture. *Soufleris et al.* [1982] interpreted each cluster as being associated with an event: the eastern one, the main shock, the central one, the main foreshock (May 23, 1978, M_s = 5.7); and the western one, a small aftershock (August 21, 1978, m_b = 4.2). We now doubt the details of that interpretation. If we allow 16 km of the fault to slip 0.70 m, this explains the distribution of 83% of the aftershocks. We therefore adopt this model, although for the purposes of looking at more distant Coulomb stress interactions, this is not very important.

A26. December 19, 1981 (1981.1), Aegean Earthquake; M_s=7.2; Q=D

This event occurred in the Aegean Sea, on the southern edge of the Skyros Basin. The focal mechanism [*Taymaz et al.*, 1991; *Kiratzi et al*., 1991] indicated right-lateral strike-slip faulting striking northeast-southwest, parallel to the orientation of the southern branch of the North Anatolian fault. The aftershock sequence also defined a northeast-southwest trend [*Taymaz et al*., 1991]. This earthquake is very similar to the 1968 strike-slip earthquake which occurred on the other edge of the Skyros Basin. We model as this event with a length of 60 km and a mean displacement of 3.2 m (using KA).

A27. December 27, 1981 (1981.2), Aegean Earthquake; M_s=6.4; Q=D

This event occurred at the southwest extremity of the Skyros Basin 8 days after the 1981.1 event and could be considered to be a strong aftershock. Its focal mechanism also indicates right-lateral faulting striking northeast-southwest [*Taymaz et al*., 1991]. We model it as a right-lateral fault with a length of 16 km and a displacement of 0.75 m (using KA).

A28. January 18, 1982, Aegean Earthquake; M_s=6.9; Q=D

This event occurred in the Aegean Sea in the central part of the North Aegean Trough. The focal mechanism indicates right-lateral strike-slip faulting on a northeast-southwest plane [*Taymaz et al*., 1991; *Kiratzi et al*., 1991]. The aftershock zone was elongated to the northeast like the North Anatolian Fault in the area [*Taymaz et al*., 1991]. It is not clear if that event was located on the northern or southern edge of the North Aegean Trough. However, the more prominent strike-slip fault is located on the southern edge, and the aftershocks are concentrated there. We therefore place the event along this edge with a length of 30 km and displacement of 2.25 m (using KA)

A29. August 6, 1983, Aegean Earthquake; M_s=6.9; Q=D

This event occurred in Aegean Sea, just east of the previous one. The northeast elongation of the aftershock zone and the strike-slip focal mechanism are similar to the 1982 earthquake [*Taymaz et al*., 1991; *Kiratzi et al*., 1991]. We model it as a northeast-southwest right-lateral fault on the southern edge of the North Aegean Trough with a similar length of 30 km and a displacement of 2.25 m (using KA).

Acknowledgments. We greatly appreciate the help of A. Barka, Ö. Alptekin and of A.O. Öncel. This work was supported by the Research Fund of Istanbul University under project numbers: 785/131295, Ö-III/25, YP/25/140789. A part of the study also supported by TÜBITAK, NATO A-2 scholarship given to S. Nalbant. Support was also received from the PNRN program of INSU-CNRS and from project FAUST funded by DGXII of the European Community. This is IPGP contribution number 1557.

References

Aki, K., and P. G. Richards, Quantitative Seismology, W.H. Freeman, New York, 1980.
Ambraseys, N.N., Some characteristic features of the North Anatolian fault zone, *Tectonophysics*, *9*, 143-165, 1970.
Ambraseys, N.N. (1988). Engineering seismology, *Earthquake Eng. Struct. Dyn., 17*, 1-105.
Ambraseys, N.N., and C. Finkel, The Saros-Marmara earthquake of 9 August 1912, *Earthquake Eng. Struct. Dyn., 15*,

, J. Geophys. Res., 103, 24469-24486

189-211, 1987.
Ambraseys, N.N., and C. Finkel, Long-term seismicity of Istanbul and of the Sea Marmara region, *Terra Nova*, *3*, 527-539, 1991.
Ambraseys, N.N., and J.A. Jackson, Seismicity and associated strain of central Greece between 1890 and 1988, *Geophys. J. Int*., *101*, 663-708, 1990.
Ambraseys , N.N., and J.S. Tchalenko, Seismotectonic aspects of the Gediz, Turkey, earthquake of March 1970, *Geophys. J. R. Astron. Soc*., *30*, 229-252, 1972.
Ambraseys, N.N., and A. Zatopek, The Mudurnu valley, west Anatolia, Turkey, earthquake of 22 July 1967, *Bull. Seismol. Soc. Am*., *59*, 521-589, 1969.
Ambraseys, N.N., A. Zatopek, M. Tasdemiroglu and A. Aytun, The Mudurnu valley, West Anatolia earthquake of 22 July 1967, *Publ., 22/BMS*, 135 pp, UNESCO, Geneva, 1968.
Angelier, J., J.F. Dumont, H. Karamanderesi, A. Poisson, S. Simsek, and S. Uysal, Analysis of fault mechanisms and extensions of southwestern Anatolia since late Miocene, *Tectonophysics*, *75*, T1-T9, 1981.
Armijo, R., B. Meyer, G.C.P. King A. Rigo, and D. Papanastassiou, Quaternary evolution of the Corinth rift and its implications for the late Cenozoic evolution of the Aegean, *Geophys. J. Int*., *126*, 11-53, 1996.
Arpat, E., and E. Bingöl, The rift system of Western Turkey, throught on its development, *Bull. Miner. Res. Expl. I*., *73*, 1-9, 1969.
Ates, R., Earthquake activity on the North Anatolian Fault Zone, in *Progress in Earthquake Prediction*, edited by A.M. Isikara and A. Vogel, pp. 95-113, Vieweg and john, Wiesbaden, Germany, 1982.
Ates, R., and A. Tabban, A preliminary report on August 9, 1912 Mürefte-Sarköy earthquake (in Turkish), *Earthquake Res. Inst*., Ankara, Turkey, 1976.
Barka, A.A., The North Anatolian fault zone, *Ann. Tectonicae*, suppl. *VI*, 164-195, 1992.
Barka, A.A., Slip distribution along the North Anatolian fault associated with the large earthquakes of the period 1939 to 1967, *Bull. Seismol. Soc. Am*., *86*, 1238-1254, 1996.
Barka, A.A., and K. Kadinsky-Cade, Strike-slip fault geometry in Turkey and its influence on earthquake activity, *Tectonophysics*, *7*, 663-684, 1988.
Burov, E.B., and M. Diament, Flexure of the continental lithosphere with multilayer rheology, *Geophys. J. Int*., *109*, 440-468, 1992.
Canitez, N., Source mechanism and rupture propagation in the Mudurnu Valley, Turkey, earthquake of July 22, 1967, *Pure Appl. Geophys*., *93*, 116-124, 1972.
Deng, J., and L.R. Sykes, Evolution of the stress Field in Southern California and triggering of moderate-size earthquakes: A 200-year perspective, *J. Geophys. Res*., *102*, 9859-9886, 1997.
Ellis, M.A., and G.C.P. King, Structural control of flank volcanism in continental rifts, *Science*, *254*, 839-842, 1990.
Erentöz, C., and F. Kurtman, A report on the 1964 Manyas earthquake (in Turkish), *Bull. Miner. Res. Expl. I*., *63*, 1-5, 1965.
Ergin, K., U. Güçlü, and Z. Uz, An earthquake catalogue for Turkey and surrounding regions (MS 11-1964). *Publ. 24*, 189 pp., Earth Phys. Inst., *Istanbul Tech. Univ., Min. Fac*., Istanbul, 1967.
Eyidogan, H., and J. Jackson, A seismological study of normal faulting in the Demirci, Alasehir and Gediz earthquakes of 1969-70 in western Turkey: Implications for the nature and geometry of deformation in the continental crust, *Geophys. J. R. Astron. Soc*., *81*, 569-607, 1985.
Eyidogan, H., U. Güçlü, Z. Utku, and E. Degirmenci, A Macro-seismic Guide for Large Earthquakes of Turkey (1900-1988) (in Turkish). 198 pp., Kurdis Press, Istanbul, 1991.
Floras, D., The destructions of the Chalkidiki earthquakes, short technical report (in Greek), *Tech. Chron*., *25* (B/11), pp. 21-28, Technical Cham. Greece, Athens, 1933.
Georgalas, G., and A. Galanopoulos, The large Chalkidike earthquake of the 26 September 1932 (in German), *Delt Hell. Geol. Hetair*., *1*, 11-63, 1953.
Güçlü, U., Section 1: Field investigation (in Turkish), in *Investigations on July 22, 1967 Mudurnu valley earthquake*, Publ. 27, edited by K. Ergin, pp. 1-27, Istanbul Tech. Univ., Min. Fac., Earth Phys. Inst., Istanbul, 1969.
Harris, R.A., and R.W. Simpson, Changes in static stress on southern California faults after the 1992 Landers earthquakes, *Nature*, *360*, 251-254, 1992.
Harris, R.A., and R.W. Simpson, In the shadow of the 1857- The effect of the great Ft. Tejon earthquake on the subsequent earthquakes in southern California, *Geophys. Res. Lett*., *23*, 229-232, 1996.
Harris, R.A., R.W. Simpson, and P.A. Reasenberg, Influence of static stress changes on earthquake locations in southern California, *Nature*, *375*, 221-224, 1995.
Hodgkinson, M.K., R.S. Stein, and G.C.P. King, The 1954 Rainbow Mountain-Fairview Peak-Dixie valley earthquakes: A triggered normal faulting sequence, *J. Geophys. Res*., *101*, 25459-25471, 1996.
Jackson, J., and T.J. Fitch, Seismotectonic implications of relocated aftershock sequence in Iran and Turkey, *Geophys. J. R. Astron. Soc*., *57*, 209-229, 1979.
Jackson J., and D.P. McKenzie, Active tectonics of the Alpine-Himalayan Belt between western Turkey and Pakistan, *Geophys. J. R. Astron. Soc*., *77*, 185-246, 1984.
Jackson J., and D.P. McKenzie, The relationship between plate motion and seismic moment tensors, and the rates of active deformation in the Mediterranean and Middle East, *Geophys. J*., *93*, 45-73, 1988.
Jacques, E., G.C.P. King, P. Tapponnier, J.C. Ruegg, and I. Manighetti, Seismic activity triggered by stress changes after the 1978 events in the Asal Rift, Djibouti, *Geophys. Res. Lett*., *23*, 2481-2484, 1996.
Jaumé, S.C., and L.R. Sykes, Evolution of the moderate seismicity in the San Francisco Bay region, 1850 to 1993: Seismicity changes related to the occurrence of large and great earthquakes, *J. Geophys. Res*., *101*, 765-789, 1996.
Kanamori, H., and D.L. Anderson, Theoretical basis of some empirical relations in seismology, *Bull. Seismol. Soc. Am*., *65*, 1073-1095, 1975.
Ketin, I., Tension cracks occurred on the surface during the October 6, 1964 Manyas earthquake (in Turkish), *Bull. Turk. Geol. Union*, *10*, 44-51, 1966.
Ketin, I., About the strike-slip movement of North Anatolia (in German), *Bull. Miner. Res. Explor. Inst. Turkey*, *72*, 1-28, 1969.
Ketin, I., and S. Abdüsselamoglu, Macro-seismic observations on March 23, 1969 Demirci and March 28, 1969 Alasehir-Sarigöl earthquakes (in Turkish*), Min. Mag. Istanbul Univ*., *4* (5), 21-26, 1969.
Ketin, I., and T. Roesli, Macroseismic research of the Northwest Anatolian earthquake of the 18 March 1953 (in German), *Eclogae Geol. Helv*., *46*, 187-208, 1953.
King, G.C.P., Z.X. Ouyang, P. Papadimitriou, A. Deschamps, J. Gagnepain, G. Houseman, J.A. Jackson, C. Soufleris, and J. Virieux, The evolution of the Gulf of Corinth (Greece): An aftershock study of the 1981 earthquakes, *Geophys. J. R. Astron. Soc*., *80*, 677-683, 1985.
King, G.C.P., R.S. Stein, and J.B. Rundle, The growth of geological structures by repeated earthquakes, 1, Conceptual framework, *J. Geophys. Res*., *93*, 13307-13318, 1988.

King, G.C.P., D. Oppenheimer, and F. Amelung, Block versus continuum deformation in the western United States, *Earth Planet. Sci. Lett., 128*, 55-64, 1994a.
King, G.C.P., R.S. Stein, and J. Lin, Static stress changes and the triggering of earthquakes, *Bull. Seismol. Soc. Am., 84*, 935-953, 1994b.
Kiratzi, A., G. Wagner, and C. Langston, Source parameters of some large earthquake in North Aegean determined by body waveform inversion, *Pure Appl. Geophys., 135*, 515-527, 1991.
Kusznir, N.J., G. Marsden, and S.S. Egan, A flexural cantilever simple shear/pure shear model of continental lithosphere extension: Applications to the Jeanne d'Arc basin, and the Viking graben, North Sea, in *The Geometry of Normal Faults*, edited by Robert, A.M., G. Yielding, and B. Freeman, *Geol. Soc. Spec. Publ., London, 56*, 41-60, 1991.
Macovei, G., About the Sea of Marmara earthquake of the 9 August 1912 (in French), *Bull. Sect. Sci. Acad. Roumanie, Bucarest, 1* (1), pp. 1-10, 1912.
Maravelakis, M., Geological and macroseismical characteristics of the Chalkidiki earthquake (September 1932) (in Greek). Thesis, Univ. of Thessaloniki, Thessaloniki, Greece, 1933.
McKenzie, D.P., Active tectonics of the Mediterranean region, *Geophys. J. R. Astron. Soc., 30*, 109-185, 1972.
Mercier, J.L., N. Mouyaris, C. Simeakis, T. Roundoyannis, and C. Angelidhis, Intra-plate deformation: A quantitative study of the fault activated by the 1978 Thessaloniki earthquake, *Nature, 278*, 45-48, 1979.
Mihailovic, J., The large seismic disasters around the Sea of Marmara (in French), Inst. Seismol. de l'Univ. de Belgrade, Belgrade, Yugoslavia, 1927.
Mihailovic, J., The seismicity of the, the Sea of Marmara and of Asia minor (in French), *Monogr. Trav. Sci. Inst. Seismol., 2B*, 1933.
Muir-Wood, R., and G.C.P. King, Hydrological signature of earthquake strain, *J. Geophys. Res., 98*, 22035-22068, 1993.
Müller, B., M.L. Zoback, K. Fuchs, L. Mastin, S. Gregersen, N. Pavoni, Stephansson, and C. Ljunggren, Regional patterns of tectonic stress in Europe, *J. Geophys. Res., 97*, 11783-11803, 1992.
Nalbant, S.S., A.A. Barka, and Ö. Alptekin, Failure stress change caused by the 1992 Erzincan earthquake (Ms=6.8), *Geophys. Res. Lett., 23*, 1561-1564, 1996.
North, R.D., Seismic moment, source dimension, and stresses associated with 23 March 1969 earthquake, *Geophys. J. R. Astron. Soc., 48*, 137-161, 1977.
Nostro, C., M. Cocco, and M.E. Belardinelli, Static stress changes in extensional regimes: An application to Southern Apennines (Italy), *Bull. Seismol. Soc. Am., 87*, 234-248, 1997.
Öcal, N., Macroseismic and microseismic investigations of February 20, 1956 Eskisehir earthquake (in Turkish). Istanbul Tech. Univ., Seismol. Inst., Istanbul, 1959a.
Öcal, N., May 26, 1957 Abant earthquake (in Turkish), *Seismol. Publ., 4*, 70 pp., Kandilli Obs., Istanbul, 1959b.
Öcal, N., S.B. Uçer, and D. Taner, Manyas-Karacabey earthquake of October 6, 1964 (in Turkish),), *Seismol. Publ., 11*, Kandilli Obs., Istanbul, 1968.
Oral, B.M., R.R. Reilinger, M.N. Toksöz, R.W. King, A.A. Barka, I. Kinik, and O. Lenk, Global positioning system offers evidence of plate motions in Eastern Mediterranean, *Eos Trans. AGU, 76*, 9-11, 1995.
Öztin, F., August 9, 1912 Mürefte-Sarköy earthquake (in Turkish), *Bull. 56*, pp. 91-127, Earthquake Res. Inst., Ankara, Turkey, 1987.
Pamir, H., F. Baykal, and I. Ketin, A geological report on Adapazari-Hendek earthquake (20.06.1943) (in Turkish), report, Earthquake Res. Inst., Ankara, Turkey, 1943.
Pavlides, S.B., and M.D. Tranos, Structural characteristics of two strong earthquake in North Aegean: Ierissos (1932) and Agios Efstratios (1968), *J. Struct. Geol., 13*, 205-214, 1991.
Pinar, N., The Yenice earthquake of the 18 March 1953 and the fracture line of Yenice-Gönen, *Rev. Fac. Sci. Univ. Istanbul, Ser. A, 18*, 131-141, 1952.
Pinar, N., and E. Lahn, Earthquake Catalogue for Turkey (in Turkish); *Bayindirlik Bakanligi, 36* (6), Yapi Imar Isleri Reisligi, Ankara, Turkey, 1952.
Reasenberg, P.A., and R.W., Simpson, Response of regional seismicity to the static stress change produced by the Loma Prieta earthquake, *Science, 255*, 1687-1690, 1992.
Rebai, S., H. Philip, and A. Taboada, Modern tectonic stress field in the Mediterranean region: evidence for variation in stress direction at different scales, *Geophys. J. Int., 110*, 106-140, 1992.
Reilinger, R.E., S.C. McClusky, M.B. Oral, R.W. King, M.N. Toksöz, A.A. Barka, I. Kinik, O. Lenk, and I. Sanli, Global Positioning System measurements of the present-day crustal movements in the Arabia-Africa-Eurasia plate collision zone, *J. Geophys. Res., 102*, 9983-9999, 1997.
Ritsema, A.R., The earthquake mechanism of the Balkan region, *Sci. Rep. 74-4*, pp. 1-36, R. Neth. Meteorol. Inst., De Bilt, 1974.
Roesli, T., A report on 18/3/53 Gönen-Yenice and 18/6/53 Edirne earthquakes (in Turkish), report, Istanbul Tech. Univ., Seismol. Inst., Istanbul, 1953.
Soufleris, C., and G.C.P. King, A source study of the largest foreshock (on May 23) and the mainshock (on June 20) of the Thessaloniki 1978 sequence, *in The Thessaloniki 1978 Earthquakes*, edited by B.C. Papazachos and P. Carydis, pp. 201-222, Dep. of Earth Sci., Univ. of Thessalonoki, Thessalonoki, Greece, 1981.
Soufleris, C., and G.S. Stewart, A source study of the Thessaloniki (northern Greece) 1978 earthquake sequence, *Geophys. J. Astron. Soc., 67*, 343-358, 1981.
Soufleris, C., J.A. Jackson, G.C.P. King, C.P. Spencer, and C.H. Scholz, The 1978 earthquake sequence near Thessaloniki (northern Greece), *Geophys. J. Astron. Soc., 68*, 429-458, 1982.
Stein, R.S., G.C.P King, and J.B. Rundle, The growth of geological structures by repeated earthquakes, 2, Field examples of continental dip-slip faults, *J. Geophys. Res., 95*, 13319-13331, 1988.
Stein, R.S., G.C.P. King, and J. Lin, Change in failure stress on the southern San Andreas fault system caused by the 1992 magnitude = 7.4 Landers earthquake, *Science, 258*, 1328-1332, 1992.
Stein, R.S., G.C.P. King, and J. Lin, Stress triggering of the 1994 *M*=6.7 Northridge, California, earthquake by its predecessors, *Science, 265*, 1432-1435, 1994.
Stein, R.S., A.A. Barka, and J.H. Dieterich, Progressive failure on the North Anatolian fault since 1939 by earthquake stress triggering, *Geophys. J. Int., 128*, 594-604, 1997.
Stewart S.G., and H. Kanamori, Complexity of rupture in large strike-slip earthquakes in Turkey, *Phys. Earth Planet. Inter., 28*, 70-84, 1982.
Straub, C., Recent crustal deformation and strain accumulation in the Marmara Sea region, N.W. Anatolia, inferred from GPS measurements, Ph.D. thesis, Swiss Fed. Inst. of Technol., Zurich, 1996.
Straub, C., and H.G. Khale, Global positioning System (GPS) estimates of crustal deformation in the Sea of Marmara region, northwestern Anatolia, *Earth Planet Sci. Lett., 121*, 495-502, 1994.
Straub, C. and H.G. Khale, Active crustal deformation in the Sea of Marmara region, NW Anatolia, inferred from GPS measurements, *Geophys. Res. Lett., 22*, 2533-2536, 1995.
Taymaz, T., J. Jackson, and D. McKenzie, Active tectonics of the north and central Aegean Sea, *Geophys. J. Int., 106*,

433-490, 1991.
Westaway, R., Block rotation in western Turkey, 1, Observational evidence, *J. Geophys. Res*., *95*, 19857-19884, 1990.
Westaway, R., Neogene evolution of the Denizli region of western Turkey, *J. Struct. Geol*., *15*, 37-53, 1993.
Wong, H.K., T. Lüdmann, A. Ulug, and N. Görür, The sea of Marmara: A plate boundary sea in an escape tectonic regime, *Tectonophysics*, *244*, 231-250, 1995.
Yaltirak, C., The tectonic history of the Ganos Fault System, *Bull. Turk. Assoc. Petroleum Geol*., *8*, 137-150, 1996.
Zanchi, A., and J. Angelier, Seismotectonics of western Anatolia: regional stress orientation from geophysical and geological data, *Tectonophysics*, *222*, 259-274, 1993.

A. Hubert, G.C.P. King, Laboratoire de Tectonique et Mécanique de la Lithosphère (UMR 7578 CNRS), Institut de Physique du Globe, 4 Place Jussieu, 75252 Paris, Cedex 05, France (e-mail: king@ipgp.jussieu.fr)
S.S. Nalbant, Geophysics Department, Engineering Faculty, Istanbul University, 34850 Avcilar, Istanbul, Turkey (e-mail: snalbant@istanbul .edu.tr)

(Received June 12, 1997; revised April 7, 1998;
accepted April 28, 1998.)